Available online at www.sciencedirect.com
ScienceDirect
Comput. Methods Appl. Mech. Engrg. 373 (2021) 113469
Computer methods in applied mechanics and engineering
www.elsevier.com/locate/cma

Coupling Arbogast–Correa and Bernardi–Raugel elements to resolve coupled Stokes–Darcy flow problems

Graham Harper[a], Jiangguo Liu[b,*], Simon Tavener[b], Tim Wildey[c]

[a] Center for Computing Research, Computational Mathematics Department, Sandia National Laboratories, Albuquerque, NM 87185-1318, USA
[b] Department of Mathematics, Colorado State University, Fort Collins, CO 80523-1874, USA
[c] Center for Computing Research, Optimization and UQ Department, Sandia National Laboratories, Albuquerque, NM, 87185-1318, USA

Received 29 March 2020; received in revised form 3 September 2020; accepted 23 September 2020
Available online 13 October 2020

Abstract

This paper presents a finite element method for solving coupled Stokes–Darcy flow problems by combining the classical Bernardi–Raugel finite elements and the recently developed Arbogast–Correa (AC) spaces on quadrilateral meshes. The novel weak Galerkin methodology is employed for discretization of the Darcy equation. Specifically, piecewise constant approximants separately defined in element interiors and on edges are utilized to approximate the Darcy pressure. The discrete weak gradients of these shape functions and the numerical Darcy velocity are established in the lowest order AC space. The Bernardi–Raugel elements (BR_1, Q_0) are used to discretize the Stokes equations. These two types of discretizations are combined at an interface, where kinematic, normal stress, and the Beavers–Joseph–Saffman (BJS) conditions are applied. Rigorous error analysis along with numerical experiments demonstrate that the method is stable and has optimal-order accuracy.

Keywords: Arbogast–Correa spaces; Bernardi–Raugel elements; Darcy flow; Quadrilateral meshes; Stokes flow; Weak Galerkin (WG)

1. Introduction

Many biological and engineering applications involve the coupling of free flow and porous-medium flow across an interface. These applications include flow of oil through a porous filter medium, pollutant transport in rivers, chemical transport in blood vessels, and food processing, just to name a few. Mathematically, such phenomena can be modeled by the coupling of the standard Stokes equations or time-dependent Stokes equations or Navier–Stokes equations with the Darcy equation (steady-state or time-dependent) [1–6] across known interfaces, for which conservation of mass, balance of forces, and the Beavers–Joseph–Saffman (BJS) condition are specified [7,8]. Specifically, cross-flow membrane filtration was investigated in [9], problems with highly heterogeneous permeability were investigated in [10]. In this paper, we focus on the coupling of the steady-state Stokes and Darcy equations.

Development of efficient and stable numerical solvers for Stokes–Darcy problems has been attracting a great deal of attention from researchers in the communities of numerical analysis and scientific computing [11–16] (and

* Corresponding author.
E-mail addresses: gbharpe@sandia.gov (G. Harper), liu@math.colostate.edu (J. Liu), tavener@math.colostate.edu (S. Tavener), tmwilde@sandia.gov (T. Wildey).

https://doi.org/10.1016/j.cma.2020.113469
0045-7825/

references therein). There are a variety of finite element solvers for Stokes flow or Darcy flow independently, and not all combinations are appropriate for the coupled problem. The main issue is incorporating these finite element discretizations with the interface conditions, especially the BJS condition.

Note that the Stokes problem is usually stated as a mixed variational formulation, whereas the Darcy part may be written in the primal or mixed formulation. When both parts are in the mixed variational formulations, conforming mixed finite element methods can be developed [17–19].

In [20], divergence-conforming finite elements for the velocities were used for the whole domain, along with hybridizable discontinuous Galerkin (HDG) for Stokes discretization and mixed finite elements for Darcy discretization. In [21], the velocity is discretized by an $H(\mathrm{div})$ virtual element, whereas the pressure is approximated by discontinuous piecewise polynomials. This allows general polygonal meshes. The weak Galerkin (WG) finite element methods developed in [22,23] allow general polygonal meshes also, but the discrete velocity is not in an $H(\mathrm{div})$-conforming subspace.

Mortar finite element methods have been developed to allow non-matching grids on the interface [10,17,24]. The majority of existing methods are established in the monolithic way, but iterative coupling of Stokes and Darcy solvers has been studied [10,25]. Additionally, for the Stokes part, there are approaches other than the traditional velocity–pressure formulation. A new formulation based on stress, vorticity, and velocity was used in [26].

In this paper, we develop an efficient finite element method for coupled Stokes–Darcy flow problems. We intend to have the least unknowns while maintaining flexibility in accommodation of complicated domain geometry, so we consider quadrilateral meshes (extension to hexahedral meshes is basically technical). We use the Bernardi–Raugel element pair (BR_1, Q_0) for Stokes flow [27] and the newly designed weak Galerkin $(P_0, P_0; AC_0)$ finite element for Darcy flow [28]. Rigorous analysis along with numerical experiments are presented to demonstrate the optimal-order accuracy and efficiency of this new solver. The following factors have been taken into consideration in the development of this new method.

(i) Compared to simplicial (triangular and tetrahedral) meshes, quadrilateral and hexahedral meshes are equally flexible in accommodation of complicated domain geometry but usually involve less degrees of freedom. For many applications, quadrilateral and hexahedral meshes perform well in alignment of geometric and physical features of the problems to be solved.
(ii) The classical Bernardi–Raugel finite element pair (BR_1, Q_0) (for Stokes flow) and the relatively new Arbogast–Correa spaces (for elliptic problems) are designed for general convex quadrilaterals.
(iii) By utilizing the Arbogast–Correa spaces for discrete weak gradients and the numerical Darcy velocity, the weak Galerkin finite element $(P_0, P_0; AC_0)$ serves as an efficient Darcy solver with the least unknowns.
(iv) When WG$(P_0, P_0; AC_0)$ for Darcy flow is coupled with (BR_1, Q_0) for Stokes flow, the Darcy pressure unknowns on the interface edges behave similarly to Lagrange multipliers. This new feature brings simplicity and clarity to the error analysis.

The rest of this paper is organized as follows. Section 2 states the problem, interface conditions, and variational formulation. Sections 3 and 4 discuss the properties of the Bernardi–Raugel and Arbogast–Correa spaces, respectively. Section 5 presents our new finite element scheme for the coupled flow problem. Section 6 starts with several lemmas and then presents a rigorous analysis for the new finite element scheme. Section 7 provides numerical verification. Section 8 concludes with some remarks.

2. The coupled Stokes–Darcy flow problem

Let $\Omega = \Omega^{\mathcal{S}} \cup \Omega^{\mathcal{D}}$ be a nonoverlapping domain decomposition, where $\Omega^{\mathcal{S}}$, $\Omega^{\mathcal{D}}$ are bounded polygonal domains for Stokes flow and Darcy flow, respectively. Furthermore, let
– $\Gamma_D^{\mathcal{S}}, \Gamma_N^{\mathcal{S}}$ be the Dirichlet and Neumann boundaries for the Stokes flow;
– $\Gamma_D^{\mathcal{D}}, \Gamma_N^{\mathcal{D}}$ be the Dirichlet and Neumann boundaries for the Darcy flow;
– $\Gamma^{\mathcal{I}}$ be the Stokes–Darcy interface.

For the Stokes flow, we consider the unknown velocity and pressure $(\mathbf{u}^{\mathcal{S}}, p^{\mathcal{S}})$, then the strain tensor $\varepsilon(\mathbf{u}^{\mathcal{S}}) = \frac{1}{2}(\nabla \mathbf{u}^{\mathcal{S}} + (\nabla \mathbf{u}^{\mathcal{S}})^T)$ and the Cauchy stress tensor $\sigma = 2\mu\varepsilon(\mathbf{u}^{\mathcal{S}}) - p^{\mathcal{S}}\mathbf{I}$, where $\mathbf{I}$ is the order-2 identity matrix and μ

is the constant dynamic viscosity. The governing equations and boundary conditions are

$$\begin{cases} -\nabla\cdot\sigma = \mathbf{f} \quad \text{in} \quad \Omega^{\mathcal{S}}, \\ \nabla\cdot\mathbf{u}^{\mathcal{S}} = 0 \quad \text{in} \quad \Omega^{\mathcal{S}}, \\ \mathbf{u}^{\mathcal{S}} = \mathbf{u}_D^{\mathcal{S}} \quad \text{on} \quad \Gamma_D^{\mathcal{S}}, \\ \sigma\mathbf{n}^{\mathcal{S}} = \mathbf{t}_N^{\mathcal{S}} \quad \text{on} \quad \Gamma_N^{\mathcal{S}}, \end{cases} \tag{1}$$

where $\mathbf{f}$ is a given body force.

For the Darcy flow, we consider $p^{\mathcal{D}}$ as the unknown pressure, $\mathbf{K} = \mu^{-1}\mathbf{k}$ a known permeability matrix where $\mathbf{k}$ is the usual hydraulic permeability tensor, $\mathbf{f}^{\mathcal{D}}$ a known extra term due to gravity or alike, s a source. The governing equation and boundary conditions are

$$\begin{cases} \nabla\cdot(-\mathbf{K}(\nabla p^{\mathcal{D}} - \mathbf{f}^{\mathcal{D}})) \equiv \nabla\cdot\mathbf{u}^{\mathcal{D}} = s \quad \text{in} \quad \Omega^{\mathcal{D}}, \\ p^{\mathcal{D}} = p_D^{\mathcal{D}} \quad \text{on} \quad \Gamma_D^{\mathcal{D}}, \\ \mathbf{u}^{\mathcal{D}}\cdot\mathbf{n}^{\mathcal{D}} = u_N^{\mathcal{D}} \quad \text{on} \quad \Gamma_N^{\mathcal{D}}. \end{cases} \tag{2}$$

A fundamental issue in the coupling of Stokes and Darcy flows arises during the formulation of interface conditions. We adopt three interface conditions on $\Gamma^{\mathcal{I}}$ as follows [4,7,8,22,24].

(i) *Conservation of mass*:

$$\mathbf{u}^{\mathcal{S}}\cdot\mathbf{n}^{\mathcal{S}} = -\mathbf{u}^{\mathcal{D}}\cdot\mathbf{n}^{\mathcal{D}}. \tag{3}$$

(ii) *Balance of normal forces*:

$$\sigma\mathbf{n}^{\mathcal{S}}\cdot\mathbf{n}^{\mathcal{S}} = -p^{\mathcal{D}}. \tag{4}$$

(iii) *Beavers–Joseph–Saffman (BJS) condition*:

$$\sigma\mathbf{n}^{\mathcal{S}}\cdot\mathbf{t}^{\mathcal{S}} = -\frac{\mu\alpha}{\sqrt{\mathbf{k}\mathbf{t}^{\mathcal{S}}\cdot\mathbf{t}^{\mathcal{S}}}}\mathbf{u}^{\mathcal{S}}\cdot\mathbf{t}^{\mathcal{S}}, \tag{5}$$

where α is an experimentally determined dimensionless coefficient that depends only on the properties of the porous medium, and $\mathbf{k}$ is the hydraulic permeability defined above. Mathematically, α is assumed to be smooth and have positive upper and lower bounds [4,7,8].

Note that, the BJS condition contains the permeability component in the tangential direction on the interface, but does not involve Darcy pressure or velocity.

As usual, we use $H^1(\Omega^{\mathcal{S}})$, $\mathbf{H}^1(\Omega^{\mathcal{S}})$, $\mathbf{H}^2(\Omega^{\mathcal{S}})$ to denote respectively the Sobolev spaces of scalar- and vector-valued functions defined on $\Omega^{\mathcal{S}}$. Similarly, $H^1(\Omega^{\mathcal{D}})$ is used to denote the Sobolev space of scalar-valued functions defined on $\Omega^{\mathcal{D}}$. Furthermore, let $\mathbf{H}^1_{0,\Gamma_D^{\mathcal{S}}}$ be the subspace of functions in $\mathbf{H}^1(\Omega^{\mathcal{S}})$ that vanish on $\Gamma_D^{\mathcal{S}}$, and similarly, $H^1_{0,\Gamma_D^{\mathcal{D}}}$ be the subspace of functions in $H^1(\Omega^{\mathcal{D}})$ that vanish on $\Gamma_D^{\mathcal{D}}$. Then we define four bilinear forms

$$\mathcal{A}^{\mathcal{S}}(\mathbf{u}^{\mathcal{S}},\mathbf{v}) = \int_{\Omega^{\mathcal{S}}} 2\mu\,\varepsilon(\mathbf{u}^{\mathcal{S}}) : \varepsilon(\mathbf{v}) + \int_{\Gamma^{\mathcal{I}}} \beta(\mathbf{u}^{\mathcal{S}}\cdot\mathbf{t}^{\mathcal{S}})(\mathbf{v}\cdot\mathbf{t}^{\mathcal{S}}), \tag{6}$$

$$\mathcal{B}^{\mathcal{S}}(p^{\mathcal{S}},\mathbf{v}) = \int_{\Omega^{\mathcal{S}}} p^{\mathcal{S}}(\nabla\cdot\mathbf{v}), \tag{7}$$

$$\mathcal{C}^{\mathcal{I}}(p^{\mathcal{D}},\mathbf{v}) = \int_{\Gamma^{\mathcal{I}}} p^{\mathcal{D}}(\mathbf{v}\cdot\mathbf{n}^{\mathcal{S}}), \tag{8}$$

$$\mathcal{A}^{\mathcal{D}}(p^{\mathcal{D}},q) = \int_{\Omega^{\mathcal{D}}} (\mathbf{K}\nabla p^{\mathcal{D}})\cdot\nabla q, \tag{9}$$

for $\mathbf{u}^{\mathcal{S}},\mathbf{v}\in\mathbf{H}^1(\Omega^{\mathcal{S}})$, $p^{\mathcal{S}}\in L^2_0(\Omega^{\mathcal{S}})$, and $p^{\mathcal{D}},q\in H^1(\Omega^{\mathcal{D}})$. Here $\mathbf{n}^{\mathcal{S}},\mathbf{t}^{\mathcal{S}}$ are the unit normal and tangential vectors on the interface $\Gamma^{\mathcal{I}}$ (pointing away from the Stokes domain $\Omega^{\mathcal{S}}$). Note that $\mathcal{A}^{\mathcal{S}}$ incorporates the BJS condition. Although it involves only the trial and test functions for Stokes flow, we have introduced

$$\beta = \frac{\mu\alpha}{\sqrt{(\mathbf{k}\mathbf{t}^{\mathcal{S}})\cdot\mathbf{t}^{\mathcal{S}}}}, \tag{10}$$

so it additionally involves the physical parameter $\mathbf{k}$ for Darcy flow along the interface.

Then we define two linear forms for $\mathbf{v} \in \mathbf{H}^1(\Omega^{\mathcal{S}})$ and $q \in H^1(\Omega^{\mathcal{D}})$,

$$\mathcal{F}^{\mathcal{S}}(\mathbf{v}) = \int_{\Omega^{\mathcal{S}}} \mathbf{f} \cdot \mathbf{v} + \int_{\Gamma_N^{\mathcal{S}}} \mathbf{t}_N^{\mathcal{S}} \cdot \mathbf{v}, \tag{11}$$

$$\mathcal{F}^{\mathcal{D}}(q) = \int_{\Omega^{\mathcal{D}}} s\, q - \int_{\Gamma_N^{\mathcal{D}}} u_N^{\mathcal{D}} q - \int_{\Omega^{\mathcal{D}}} (-\mathbf{K}\mathbf{f}^{\mathcal{D}}) \cdot \nabla q. \tag{12}$$

The variational formulation seeks $\mathbf{u}^{\mathcal{S}} \in \mathbf{H}^1(\Omega^{\mathcal{S}})$, $p^{\mathcal{S}} \in L_0^2(\Omega^{\mathcal{S}})$, and $p^{\mathcal{D}} \in H^1(\Omega^{\mathcal{S}})$ with $\mathbf{u}^{\mathcal{S}}|_{\Gamma_D^{\mathcal{S}}} = \mathbf{u}_D^{\mathcal{S}}$, $p^{\mathcal{D}}|_{\Gamma_D^{\mathcal{D}}} = p_D^{\mathcal{D}}$, so that

$$\begin{cases} \mathcal{A}^{\mathcal{S}}(\mathbf{u}^{\mathcal{S}}, \mathbf{v}) & -\mathcal{B}^{\mathcal{S}}(p^{\mathcal{S}}, \mathbf{v}) & +\mathcal{C}^{\mathcal{I}}(p^{\mathcal{D}}, \mathbf{v}) & = & \mathcal{F}^{\mathcal{S}}(\mathbf{v}), \\ \mathcal{B}^{\mathcal{S}}(r, \mathbf{u}^{\mathcal{S}}) & & & = & 0, \\ -\mathcal{C}^{\mathcal{I}}(q, \mathbf{u}^{\mathcal{S}}) & & +\mathcal{A}^{\mathcal{D}}(p^{\mathcal{D}}, q) & = & \mathcal{F}^{\mathcal{D}}(q), \end{cases} \tag{13}$$

for all $\mathbf{v} \in \mathbf{H}^1_{0,\Gamma_D^{\mathcal{S}}}$, $r \in L_0^2(\Omega^{\mathcal{S}})$, and $q \in H^1_{0,\Gamma_D^{\mathcal{D}}}$.

3. Discretization of Stokes flow by Bernardi–Raugel elements

3.1. Bernardi–Raugel elements (BR_1, Q_0) for quadrilaterals

Let E be a quadrilateral with vertices $P_i(x_i, y_i)(i = 1, 2, 3, 4)$ starting at the lower-left corner and going counterclockwise. Let $e_i(i = 1, 2, 3, 4)$ be the edge connecting P_i to P_{i+1} with the modulo convention $P_5 = P_1$. Let $\mathbf{n}_i(i = 1, 2, 3, 4)$ be the outward unit normal vector on edge e_i. A bilinear mapping from $(\hat{x}, \hat{y})$ in the reference element $\hat{E} = [0, 1]^2$ to (x, y) in such a generic quadrilateral is established as follows

$$\begin{cases} x = x_1 + (x_2 - x_1)\hat{x} + (x_4 - x_1)\hat{y} + ((x_1 + x_3) - (x_2 + x_4))\hat{x}\hat{y}, \\ y = y_1 + (y_2 - y_1)\hat{x} + (y_4 - y_1)\hat{y} + ((y_1 + y_3) - (y_2 + y_4))\hat{x}\hat{y}. \end{cases} \tag{14}$$

On the reference element $\hat{E}$, we have four standard bilinear functions

$$\begin{aligned} \hat{\phi}_4(\hat{x}, \hat{y}) &= (1 - \hat{x})\hat{y}, & \hat{\phi}_3(\hat{x}, \hat{y}) &= \hat{x}\hat{y}, \\ \hat{\phi}_1(\hat{x}, \hat{y}) &= (1 - \hat{x})(1 - \hat{y}), & \hat{\phi}_2(\hat{x}, \hat{y}) &= \hat{x}(1 - \hat{y}). \end{aligned} \tag{15}$$

After the bilinear mapping defined by (14), we obtain four scalar basis functions on E:

$$\phi_i(x, y) = \hat{\phi}_i(\hat{x}, \hat{y}), \quad i = 1, 2, 3, 4. \tag{16}$$

These are used to define eight node-based local basis functions for $Q_1(E)^2$:

$$\begin{bmatrix} \phi_1 \\ 0 \end{bmatrix}, \begin{bmatrix} 0 \\ \phi_1 \end{bmatrix}, \begin{bmatrix} \phi_2 \\ 0 \end{bmatrix}, \begin{bmatrix} 0 \\ \phi_2 \end{bmatrix}, \begin{bmatrix} \phi_3 \\ 0 \end{bmatrix}, \begin{bmatrix} 0 \\ \phi_3 \end{bmatrix}, \begin{bmatrix} \phi_4 \\ 0 \end{bmatrix}, \begin{bmatrix} 0 \\ \phi_4 \end{bmatrix}. \tag{17}$$

Furthermore, we define four edge-based scalar functions on $\hat{E}$:

$$\begin{aligned} \hat{\psi}_1(\hat{x}, \hat{y}) &= (1 - \hat{x})\hat{x}(1 - \hat{y}), & \hat{\psi}_2(\hat{x}, \hat{y}) &= \hat{x}(1 - \hat{y})\hat{y}, \\ \hat{\psi}_3(\hat{x}, \hat{y}) &= (1 - \hat{x})\hat{x}\hat{y}, & \hat{\psi}_4(\hat{x}, \hat{y}) &= (1 - \hat{x})(1 - \hat{y})\hat{y}. \end{aligned} \tag{18}$$

They become univariate quadratic functions on respective edges of $\hat{E}$, and for that reason they are sometimes referred to as edge-based "bubble functions". For a generic convex quadrilateral E, we utilize the bilinear mapping to define

$$\psi_i(x, y) = \hat{\psi}_i(\hat{x}, \hat{y}), \quad i = 1, 2, 3, 4. \tag{19}$$

Then we have four edge-based local basis functions on E (see Fig. 1):

$$\mathbf{b}_i(x, y) = \mathbf{n}_i\ \psi_i(x, y), \quad i = 1, 2, 3, 4. \tag{20}$$

Let $Q_1(E)^2$ be the set of vector-valued mapped bilinear functions on a quadrilateral E. Combining the $Q_1(E)^2$ functions and the bubble functions, the $BR_1(E)$ space on the quadrilateral is defined as

$$BR_1(E) = Q_1(E)^2 + \text{span}(\mathbf{b}_1, \mathbf{b}_3, \mathbf{b}_3, \mathbf{b}_4). \tag{21}$$

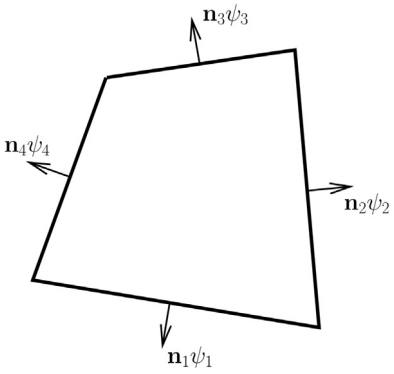

Fig. 1. Four edge-based bubble functions used in the BR_1 space.

The global finite element space is defined by combining all local spaces, but care must be taken to define the global bubble functions in a consistent manner. This may be done by defining an orientation for each edge and using that to assign a consistent direction to each bubble function's normal vector.

3.2. Properties of the (BR_1, Q_0) element pair for Stokes flow

The (BR_1, Q_0) pair satisfies several appealing properties, which will be beneficial for the approximation of Stokes flow. First, the addition of bubble functions allows for enrichment of interpolation. In [27], the global interpolation operator, denoted here as $\mathbf{P}_h$, is specified as the piecewise bilinear interpolant at mesh nodes and the bubble function coefficients are so defined that the bulk flux is captured on each edge e_i,

$$\int_{e_i} (\mathbf{P}_h\mathbf{v} - \mathbf{v}) \cdot \mathbf{n} = 0, \qquad \forall \mathbf{v} \in \mathbf{H}_0^1(\Omega). \tag{22}$$

For a polygonal domain $\Omega^{\mathcal{S}}$ and a shape-regular mesh $\mathcal{E}_h^{\mathcal{S}}$ consisting of convex quadrilaterals, this implies that for all $E \in \mathcal{E}_h^{\mathcal{S}}$,

$$(w_h, \nabla \cdot (\mathbf{P}_h\mathbf{v} - \mathbf{v}))_E = 0, \quad \forall \mathbf{v} \in \mathbf{H}_0^1(\Omega), \quad \forall w_h \in Q_0(E). \tag{23}$$

Another property described in [27] is the inf–sup condition. Let $\mathbf{V}_h$ be the global BR_1 finite element space on the mesh $\mathcal{E}_h^{\mathcal{S}}$ and let $\mathbf{V}_h^0$ be the space of functions in $\mathbf{V}_h$ that vanish on all boundaries. Then the discretization satisfies the inf–sup condition

$$\gamma \|w_h\|_{L^2(\Omega^{\mathcal{S}})} \leq \sup_{\mathbf{v} \in \mathbf{V}_h^0} \frac{(w_h, \nabla \cdot \mathbf{v}_h)_{\Omega^{\mathcal{S}}}}{\|\varepsilon(\mathbf{v}_h)\|_{L^2(\Omega^{\mathcal{S}})}}, \qquad \forall w_h \in Q_0(\mathcal{E}_h^{\mathcal{S}}), \tag{24}$$

where $\gamma > 0$ is a constant independent of mesh size h.

4. Discretization of Darcy flow by WG(P_0, P_0; AC_0) elements

Compared to the continuous and discontinuous Galerkin methods, weak Galerkin finite element methods are relatively new but have some noticeable features. For the Darcy equation, WG methods can be established based on the primal formulation but possess local mass conservation and normal flux continuity [28–30]. WG methods use reconstructed discrete weak gradients in certain subspaces that have desired approximation properties. This approach produces a numerical Darcy velocity via post-processing based on a local L^2-projection. It avoids the hybridization procedure used in the classical mixed finite element methods. In this section, we briefly discuss the new WG method $(P_0, P_0; AC_0)$ for Darcy flow on quadrilateral meshes [28].

4.1. Lowest-order Arbogast–Correa spaces AC_0 on quadrilaterals

Compared to the classical Raviart–Thomas elements [31] or the Arnold–Boffi–Falk elements [32], the Arbogast–Correa elements constructed recently in [33] for convex quadrilaterals have better approximation properties and less degrees of freedom. The $AC_k (k \geq 0)$ spaces are constructed using both unmapped vector-valued polynomials and rational functions obtained via the Piola transformation.

Let E be a convex quadrilateral and $k \geq 0$ be an integer. The local Arbogast–Correa space on E is defined as

$$AC_k(E) = P_k(E)^2 + \mathbf{x}\widetilde{P}_k(E) + \mathbb{S}_k(E), \tag{25}$$

where $P_k(E)^2$ is the space of bivariate vector-valued polynomials defined on E with a total degree at most k, $\widetilde{P}_k(E)$ is the space of bivariate homogeneous scalar-valued polynomials with degree exactly k, and $\mathbb{S}_k(E)$ is a supplementary space of vector-valued rational functions obtained via the Piola transformation.

For convenience, we write $\mathbb{S}_k = \mathcal{P}_E\hat{\mathbb{S}}_k$, where $\mathcal{P}_E$ is the Piola transformation. Let $(\hat{x}, \hat{y})$ be the coordinates in the reference element $[0, 1]^2$. According to [33], for $k = 0$,

$$\hat{\mathbb{S}}_0 = \text{span}\{\mathbf{curl}(\hat{x}\,\hat{y})\}. \tag{26}$$

For $k \geq 1$,

$$\hat{\mathbb{S}}_k = \text{span}\{\mathbf{curl}((1-\hat{x}^2)\hat{x}^{k-1}\hat{y}),\ \mathbf{curl}(\hat{x}^{k-1}\hat{y}(1-\hat{y}^2))\}. \tag{27}$$

Roughly speaking, $P_k(E)^2$ accounts for the approximation of a vector field on a convex quadrilateral, $\mathbf{x}\widetilde{P}_k(E)$ accounts for the approximation of divergence, and $\mathbb{S}_k$ offers a divergence-free supplement.

Given these discrete spaces, we have

$$\dim(P_k^2) = (k+1)(k+2), \qquad \dim(\widetilde{P}_k) = k+1,$$

and

$$\dim(\mathbb{S}_k) = 1 \ \text{ if } \ k = 0, \qquad \dim(\mathbb{S}_k) = 2 \ \text{ if } \ k > 0.$$

If we set $s_k = \dim(\mathbb{S}_k)$, then

$$\dim(AC_k(E)) = (k+1)(k+3) + s_k. \tag{28}$$

Note that $(k+1)(k+3) = \dim(RT_k)$, namely, the dimension of the kth order Raviart–Thomas (RT) space on a triangle [31]. Thus, s_k represents the additional degrees of freedom needed for augmenting the RT space on a quadrilateral [33].

However, in this paper, only the lowest-order space AC_0 is used. More interestingly, a set of local basis functions for a general quadrilateral are

$$\begin{bmatrix} 1 \\ 0 \end{bmatrix}, \ \begin{bmatrix} 0 \\ 1 \end{bmatrix}, \ \begin{bmatrix} X \\ Y \end{bmatrix}, \ \mathcal{P}_E\begin{bmatrix} \hat{x} \\ -\hat{y} \end{bmatrix}, \tag{29}$$

where $X = x - x_c$, $Y = y - y_c$ are the normalized coordinates with (x_c, y_c) being the element center, $(\hat{x}, \hat{y})$ are the reference coordinates in the reference element $[0, 1]^2$, and $\mathcal{P}_E$ is the Piola transformation mentioned above.

We need a local projection operator $\mathbf{Q}_h$ from $L^2(E)^2$ to the space $AC_0(E)$ for any quadrilateral $E \in \mathcal{E}_h^{\mathcal{D}}$. Given $\mathbf{v} \in L^2(E)^2$, find $\mathbf{Q}_h\mathbf{v} \in AC_0(E)$ such that

$$(\mathbf{Q}_h\mathbf{v}, \mathbf{w})_E = (\mathbf{v}, \mathbf{w})_E, \qquad \forall \mathbf{w} \in AC_0(E). \tag{30}$$

For error analysis, we also need the global interpolation operator $\boldsymbol{\Pi}_h$ such that for any $\mathbf{v} \in H(\text{div}, \Omega^{\mathcal{D}})$ and any edge e in the mesh $\mathcal{E}_h^{\mathcal{D}}$, there holds

$$\langle(\boldsymbol{\Pi}_h\mathbf{v}) \cdot \mathbf{n}, 1\rangle_e = \langle\mathbf{v} \cdot \mathbf{n}, 1\rangle_e. \tag{31}$$

4.2. Weak Galerkin elements $WG(P_0, P_0; AC_0)$ on quadrilaterals

Weak Galerkin finite elements use separate basis functions in element interiors and on interelement boundaries. These basis functions are different than those basis functions used in the continuous or discontinuous Galerkin methods. We call them *discrete weak functions*.

Let $k \geq 0$ be an integer and E be a convex quadrilateral with interior E° and boundary E^∂. Let $P_k(E^\circ)$ be the space of polynomials defined in E° with degree at most k, and similarly, $P_k(E^\partial)$ be the space of piecewise polynomials defined on E^∂ with degree at most k. Let $AC_k(E)$ be the space of vector-valued polynomials discussed in the previous section.

Let $\phi = \{\phi^\circ, \phi^\partial\}$ be a discrete weak function such that $\phi^\circ \in P_k(E^\circ)$ and $\phi^\partial \in P_k(E^\partial)$. Note that ϕ° is defined for the element interior only; whereas, ϕ^∂ is defined on the element boundary only. We define $\nabla_w \phi \in AC_k(E)$ by

$$\int_E (\nabla_w \phi) \cdot \mathbf{w} = \int_{E^\partial} \phi^\partial (\mathbf{w} \cdot \mathbf{n}) - \int_{E^\circ} \phi^\circ (\nabla \cdot \mathbf{w}) \qquad \forall \mathbf{w} \in AC_k(E), \tag{32}$$

or in slightly different notation

$$(\nabla_w \phi, \mathbf{w})_E = \langle \phi^\partial, \mathbf{w} \cdot \mathbf{n} \rangle_{E^\partial} - (\phi^\circ, \nabla \cdot \mathbf{w})_{E^\circ}. \tag{33}$$

This paper focuses on the case $k = 0$. We deal with discrete weak functions that are constants separately defined in element interiors and on edges. In this case, Eq. (33) is simply a size-4 SPD linear system for each quadrilateral. Its solution contains 4 coefficients to be used for expressing $\nabla_w \phi$ as a linear combination of the local basis functions of AC_0 stated in (29).

We shall also need a local L^2-projection $Q_h = \{Q_h^\circ, Q_h^\partial\}$, where Q_h° is the L^2-projection that maps a function in $L^2(E^\circ)$ to a constant in E°, whereas Q_h^∂ is the L^2-projection that maps a function in $L^2(e)$ to a constant on e for each edge e on E^∂.

5. Combining WG(P_0, P_0; AC_0) and (BR_1, Q_0) elements for coupled Stokes–Darcy flow

This section presents the finite element scheme for the coupled problem, but first we will introduce appropriate notations and spaces.

Let $\mathcal{E}_h^\mathcal{S}, \mathcal{E}_h^\mathcal{D}$ be quasi-uniform quadrilateral meshes of $\Omega^\mathcal{S}$, $\Omega^\mathcal{D}$, respectively, with size h, and let $\Gamma_h^\mathcal{I}$ be a mesh of $\Gamma^\mathcal{I}$, which is conforming with $\mathcal{E}_h^\mathcal{S}$ and $\mathcal{E}_h^\mathcal{D}$.

Let $\mathbf{V}_h^\mathcal{S}, W_h^\mathcal{S}$ be the global BR_1 and piecewise constant spaces on $\mathcal{E}_h^\mathcal{S}$ for the unknowns $(\mathbf{u}_h^\mathcal{S}, p_h^\mathcal{S})$, respectively. Then let $V_h^\mathcal{D}$ be the WG(P_0, P_0) space on $\mathcal{E}_h^\mathcal{D}$ for the unknowns $\{p_h^{\mathcal{D},\circ}, p_h^{\mathcal{D},\partial}\}$. Furthermore, we use $\mathbf{V}_h^{\mathcal{S},0}$, $V_h^{\mathcal{D},0}$ to denote the subspaces of $\mathbf{V}_h^\mathcal{S}$, $V_h^\mathcal{D}$ consisting of functions that vanish on Dirichlet boundaries, respectively.

Now we have four discrete bilinear forms defined on these finite element spaces:

$$\mathcal{A}_h^\mathcal{S}(\mathbf{u}_h^\mathcal{S}, \mathbf{v}_h) = \sum_{E \in \mathcal{E}_h^\mathcal{S}} 2\mu \int_E \varepsilon(\mathbf{u}_h^\mathcal{S}) : \varepsilon(\mathbf{v}_h) + \sum_{e \in \Gamma_h^\mathcal{I}} \int_e \beta (\mathbf{u}_h^\mathcal{S} \cdot \mathbf{t}_e^\mathcal{S})(\mathbf{v}_h \cdot \mathbf{t}_e^\mathcal{S}), \tag{34}$$

$$\mathcal{B}_h^\mathcal{S}(p_h^\mathcal{S}, \mathbf{v}_h) = \sum_{E \in \mathcal{E}_h^\mathcal{S}} \int_E p_h^\mathcal{S} (\nabla \cdot \mathbf{v}_h), \tag{35}$$

$$\mathcal{C}_h^\mathcal{I}(p_h^\mathcal{D}, \mathbf{v}_h) = \sum_{e \in \Gamma_h^\mathcal{I}} \int_e p_h^{\mathcal{D},\partial} (\mathbf{v}_h \cdot \mathbf{n}^\mathcal{S}), \tag{36}$$

$$\mathcal{A}_h^\mathcal{D}(p_h^\mathcal{D}, q_h) = \sum_{E \in \mathcal{E}_h^\mathcal{D}} \int_E (\mathbf{K} \nabla_w p_h^\mathcal{D}) \cdot \nabla_w q_h, \tag{37}$$

and two discrete linear forms

$$\mathcal{F}_h^\mathcal{S}(\mathbf{v}_h) = \sum_{E \in \mathcal{E}_h^\mathcal{S}} \int_E \mathbf{f} \cdot \mathbf{v}_h + \sum_{e \in \Gamma_{N,h}^\mathcal{S}} \int_e \mathbf{t}_N^\mathcal{S} \cdot \mathbf{v}_h, \tag{38}$$

$$\mathcal{F}_h^\mathcal{D}(q_h) = \sum_{E \in \mathcal{E}_h^\mathcal{D}} \int_{E^\circ} s q_h^\circ - \sum_{e \in \Gamma_{N,h}^\mathcal{D}} \int_e u_N^\mathcal{D} q_h^\partial - \sum_{E \in \mathcal{E}_h^\mathcal{D}} \int_E \mathbf{Q}_h(-\mathbf{K}\mathbf{f}^\mathcal{D}) \cdot \nabla_w q_h, \tag{39}$$

where $\mathbf{Q}_h$ is the local projection from $L^2(\Omega^\mathcal{D})^2$ to the broken AC_0 space.

Our finite element scheme for the coupled Stokes–Darcy flow problem seeks $\mathbf{u}_h^{\mathcal{S}} \in \mathbf{V}_h^{\mathcal{S}}$, $p_h^{\mathcal{S}} \in W_h^{\mathcal{S}}$, and $p_h^{\mathcal{D}} \in V_h^{\mathcal{D}}$ such that $\mathbf{u}_h^{\mathcal{S}}|_{\Gamma_D^{\mathcal{S}}} = \mathbf{P}_h(\mathbf{u}_D^{\mathcal{S}})$, $p_h^{\mathcal{D}}|_{\Gamma_D^{\mathcal{D}}} = Q_h^{\partial}(p_D^{\mathcal{D}})$, and for any $\mathbf{v}_h \in \mathbf{V}_h^{\mathcal{S},0}$, $r_h \in W_h^{\mathcal{S}}$, and $q_h \in V_h^{\mathcal{D},0}$, there holds

$$\left\{\begin{array}{rrrcl} \mathcal{A}_h^{\mathcal{S}}(\mathbf{u}_h^{\mathcal{S}}, \mathbf{v}_h) & -\mathcal{B}_h^{\mathcal{S}}(p_h^{\mathcal{S}}, \mathbf{v}_h) & +\mathcal{C}_h^{\mathcal{I}}(p_h^{\mathcal{D}}, \mathbf{v}_h) & = & \mathcal{F}_h^{\mathcal{S}}(\mathbf{v}_h), \\ \mathcal{B}_h^{\mathcal{S}}(r_h, \mathbf{u}_h^{\mathcal{S}}) & & & = & 0, \\ -\mathcal{C}_h^{\mathcal{I}}(q_h, \mathbf{u}_h^{\mathcal{S}}) & & +\mathcal{A}_h^{\mathcal{D}}(p_h^{\mathcal{D}}, q_h) & = & \mathcal{F}_h^{\mathcal{D}}(q_h). \end{array}\right. \tag{40}$$

For implementation, we consider five groups of (trial and test) shape functions in the following order:
– (1) Stokes velocity: BR_1 nodal basis functions;
– (2) Stokes velocity: BR_1 edge-based bubble functions;
– (3) Stokes pressure: Q_0 elementwise constants;
– (4) Darcy pressure: P_0 constants for element interiors;
– (5) Darcy pressure: P_0 constants for edges.

Accordingly, the global stiffness matrix has five row-wise and five column-wise segments, and hence it has a total of 25 blocks. The two discrete bilinear forms $\mathcal{A}_h^{\mathcal{S}}(\cdot,\cdot)$, $\mathcal{C}_h^{\mathcal{I}}(\cdot,\cdot)$ involving the interface conditions make contributions to the (1,1)-, (1,2)-, (1,5)-, (2,1)-, (2,2)-, (2,5)-, (5,1)-, (5,2)-blocks.

Note that the assembly for each of the discrete bilinear forms $\mathcal{A}_h^{\mathcal{S}}$, $\mathcal{B}_h^{\mathcal{S}}$ and $\mathcal{A}_h^{\mathcal{D}}$ is handled almost as with the independent Stokes or Darcy problem. An important part of this implementation is the handling of the interface term $\mathcal{C}_h^{\mathcal{I}}$ and the BJS condition within the $\mathcal{A}_h^{\mathcal{S}}$ term.

After a numerical Darcy pressure $p_h^{\mathcal{D}}$ is obtained from solving the sparse monolithic system, we define the numerical Darcy velocity by postprocessing the numerical Darcy pressure by

$$\mathbf{u}_h^{\mathcal{D}} = \mathbf{Q}_h(-\mathbf{K}(\nabla_w p_h^{\mathcal{D}} - \mathbf{f}^{\mathcal{D}})). \tag{41}$$

The numerical Darcy velocity is used in the upcoming section to show the weak Galerkin discretization provides conservation properties for the flow in the Darcy domain.

6. Analysis

This section presents a rigorous analysis for the new finite element scheme. For ease presentation, we adopt the following assumptions.

(i) $\mathbf{K} = \kappa\mathbf{I}$. For analysis on Darcy solvers with a general permeability, see [34].
(ii) $\mathbf{f}^{\mathcal{D}} = \mathbf{0}$. Then $\mathbf{u}^{\mathcal{D}} = -\kappa\nabla p^{\mathcal{D}}$ and $\mathbf{u}_h^{\mathcal{D}} = -\kappa\nabla_w p_h^{\mathcal{D}}$ due to (i) and (41).
(iii) Homogeneous pure Dirichlet boundary conditions are imposed for both Stokes and Darcy parts.

We define the following energy semi-norms for $\mathbf{v}_h \in \mathbf{V}_h^{\mathcal{S}}$ and $q_h \in V_h^{\mathcal{D}}$:

$$|||\mathbf{v}_h|||_h^2 = \mathcal{A}_h^{\mathcal{S}}(\mathbf{v}_h, \mathbf{v}_h), \qquad |||q_h|||_h^2 = \mathcal{A}_h^{\mathcal{D}}(q_h, q_h), \tag{42}$$

which induce an energy semi-norm on the space $\mathbf{V}_h^{\mathcal{S}} \times V_h^{\mathcal{D}}$:

$$|||(\mathbf{v}_h, q_h)|||_h^2 = |||\mathbf{v}_h|||_h^2 + |||q_h|||_h^2. \tag{43}$$

6.1. Properties of operators and subspaces

For the Stokes part, we shall need π_h as the local L^2-projection operator from $L_0^2(\Omega)$ to $W_h^{\mathcal{S}}$.

Lemma 1 (*WG Commuting Identity*)**.** *For any $E \in \mathcal{E}_h^{\mathcal{D}}$ and any $q \in H^1(E)$, there holds*

$$\mathbf{Q}_h(\nabla q) = \nabla_w(Q_h q). \tag{44}$$

Proof. See [28,29].

Under the assumption $\mathbf{K} = \kappa\mathbf{I}$, Lemma 1 implies that

$$\mathbf{Q}_h(\mathbf{K}\nabla p^{\mathcal{D}}) = \mathbf{K}(\mathbf{Q}_h\nabla p^{\mathcal{D}}) = \mathbf{K}\nabla_w(Q_h p^{\mathcal{D}}).$$

Lemma 2 (*WG Conversion to Trace*)**.** *For any $E \in \mathcal{E}_h^{\mathcal{D}}$ and any $q_h \in V_h^{\mathcal{D}}$, there holds*

$$(\mathbf{w}, \nabla_w q_h)_E = \langle \mathbf{w} \cdot \mathbf{n}, q_h^{\partial} - q_h^{\circ} \rangle_{E^{\partial}}, \qquad \forall \mathbf{w} \in AC_0(E). \tag{45}$$

Proof. This is obtained by applying the definition of discrete weak gradient $\nabla_w q_h$, the Gauss divergence theorem, and the fact that q_h° is a constant in E°. We also extend q_h° to each edge on E^{∂} when needed.

Lemma 3 (*Lower Bound for Discrete Weak Gradient*)**.** *There holds*

$$h^{-\frac{1}{2}} \|q_h^{\partial} - q_h^{\circ}\|_{E^{\partial}} \lesssim \|\nabla_w q_h\|_E, \quad \forall E \in \mathcal{E}_h^{\mathcal{D}}, \quad \forall q_h \in V_h^{\mathcal{D},0}. \tag{46}$$

Proof. Choose $\mathbf{w} \in AC_0$ so that $(\mathbf{w} \cdot \mathbf{n})|_e = q_h^{\partial} - q_h^{\circ}|_e$ for each edge $e \subset E^{\partial}$. We apply Lemma 2 and a Cauchy–Schwarz inequality to obtain

$$\begin{aligned} \|q_h^{\partial} - q_h^{\circ}\|_{E^{\partial}}^2 &= \langle \mathbf{w} \cdot \mathbf{n}, q_h^{\partial} - q_h^{\circ} \rangle_{E^{\partial}} = (\mathbf{w}, \nabla_w q_h)_E \\ &\leq \|\mathbf{w}\|_E \, \|\nabla_w q_h\|_E \\ &\approx h^{\frac{1}{2}} \|\mathbf{w} \cdot \mathbf{n}\|_{E^{\partial}} \, \|\nabla_w q_h\|_E. \end{aligned} \tag{47}$$

For the last step, we have used an estimate similar to that in [30] Lemma 5. A cancellation of $\|q_h^{\partial} - q_h^{\circ}\|_{E^{\partial}}$ yields the desired result.

Lemma 4 (*Conservation of Mass for Darcy Flow*)**.** *For any $E \in \mathcal{E}_h^{\mathcal{D}}$, there holds*

$$\int_{E^{\partial}} \mathbf{u}_h^{\mathcal{D}} \cdot \mathbf{n} = \int_E f. \tag{48}$$

Proof. This statement is common in the literature for weak Galerkin methods for Darcy flow, but the only difference here is we choose $\mathbf{v}_h = \mathbf{0}$, $r_h = 0$, and $q_h = \{\chi_{E^{\circ}}, 0\}$ in (40). The remainder of the proof follows from applying the conversion to trace and definition of the Darcy velocity (see also [28,29]).

Lemma 5 (*Bulk Flux Continuity for Darcy Flow*)**.** *For any two elements $E_1, E_2 \in \mathcal{E}_h^{\mathcal{D}}$ which share an interior edge e, their respective local velocities $\mathbf{u}_{h,1}^{\mathcal{D}}, \mathbf{u}_{h,2}^{\mathcal{D}}$ satisfy*

$$\int_e \mathbf{u}_{h,1}^{\mathcal{D}} \cdot \mathbf{n}_1 + \int_e \mathbf{u}_{h,2}^{\mathcal{D}} \cdot \mathbf{n}_2 = 0. \tag{49}$$

Proof. This is another common statement for weak Galerkin methods for Darcy flow, and just as in Lemma 4, we choose $\mathbf{v}_h = \mathbf{0}$, $r_h = 0$, but $q_h = \{0, \chi_e\}$. The remainder of the proof may be obtained by applying a conversion to trace and definition of numerical Darcy velocity (see also [28,29]).

6.2. Existence and uniqueness

In this subsection, we prove the existence and uniqueness of the finite element scheme (40). It suffices to show the uniqueness, since the discrete linear system is finite-dimensional and square. This will be accomplished by setting the source terms to zero and then showing that all parts of the discrete solution are zero. Thus, we consider the special system

$$\begin{cases} \mathcal{A}_h^{\mathcal{S}}(\mathbf{u}_h^{\mathcal{S}}, \mathbf{v}_h) & -\mathcal{B}_h^{\mathcal{S}}(p_h^{\mathcal{S}}, \mathbf{v}_h) & +\mathcal{C}_h^{\mathcal{I}}(p_h^{\mathcal{D}}, \mathbf{v}_h) & = & 0, \\ \mathcal{B}_h^{\mathcal{S}}(r_h, \mathbf{u}_h^{\mathcal{S}}) & & & = & 0, \\ -\mathcal{C}_h^{\mathcal{I}}(q_h, \mathbf{u}_h^{\mathcal{S}}) & & +\mathcal{A}_h^{\mathcal{D}}(p_h^{\mathcal{D}}, q_h) & = & 0. \end{cases} \tag{50}$$

We set $\mathbf{v}_h = \mathbf{u}_h^{\mathcal{S}}$, $r_h = p_h^{\mathcal{S}}$, and $q_h = p_h^{\mathcal{D}}$, and sum the equations to obtain

$$|\!|\!|(\mathbf{u}_h^{\mathcal{S}}, p_h^{\mathcal{D}})|\!|\!|_h^2 = \mathcal{A}_h^{\mathcal{S}}(\mathbf{u}_h^{\mathcal{S}}, \mathbf{u}_h^{\mathcal{S}}) + \mathcal{A}_h^{\mathcal{D}}(p_h^{\mathcal{D}}, p_h^{\mathcal{D}}) = 0.$$

This immediately implies $\varepsilon(\mathbf{u}_h^{\mathcal{S}}) = \mathbf{0}$, $\mathbf{u}_h^{\mathcal{S}} \cdot \mathbf{t} = 0$, and $\nabla_w p_h^{\mathcal{D}} = \mathbf{0}$. The fact that the Dirichlet boundary in the Stokes domain is nonempty implies $\mathbf{u}_h^{\mathcal{S}} = \mathbf{0}$. The discrete inf–sup condition (24) then implies that $p_h^{\mathcal{S}} = 0$.

It remains to show that $\nabla_w p_h^{\mathcal{D}} = \mathbf{0}$ implies the numerical pressure $p_h^{\mathcal{D}}$ is zero. By Lemma 3, $\nabla_w p_h^{\mathcal{D}} = \mathbf{0}$ implies that $p_h^{\partial} = (p_h^{\circ})|_e$ on each edge e of E for any $E \in \mathcal{E}_h^{\mathcal{D}}$. It is easy to see these are all the same constant on a given E. The fact that each $E \in \mathcal{E}_h^{\mathcal{D}}$ shares an edge with another element in $\mathcal{E}_h^{\mathcal{D}}$ implies that p_h^{∂} and p_h° are the same constant over the entire mesh. Since the Dirichlet boundary for the Darcy flow is nonempty, we conclude that this constant is zero. Furthermore, from this we conclude $|||(\cdot,\cdot)|||_h$ is a norm on $\mathbf{V}_h^{\mathcal{S},0} \times V_h^{\mathcal{D},0}$.

6.3. Error equations

We split the errors of finite element solutions as discrete errors and projection errors. The discrete errors are defined as

$$\mathbf{e}_h^{\mathcal{S}} = \mathbf{P}_h \mathbf{u}^{\mathcal{S}} - \mathbf{u}_h^{\mathcal{S}}, \qquad e_h^{\mathcal{S}} = \pi_h p^{\mathcal{S}} - p_h^{\mathcal{S}}, \qquad e_h^{\mathcal{D}} = Q_h p^{\mathcal{D}} - p_h^{\mathcal{D}}. \tag{51}$$

The projection errors are defined as

$$\mathbf{u}^{\mathcal{S}} - \mathbf{P}_h \mathbf{u}^{\mathcal{S}}, \qquad p^{\mathcal{S}} - \pi_h p^{\mathcal{S}}, \qquad p^{\mathcal{D}} - Q_h p^{\mathcal{D}}.$$

In this subsection, we establish error equations to express the above discrete errors in terms of the projection errors, which are known to be controlled by the regularity of the exact solutions and the approximation capacity of the finite element subspaces constructed.

Lemma 6 (*Error Equations*)**.** *Let* $(\mathbf{u}^{\mathcal{S}}, p^{\mathcal{S}}, p^{\mathcal{D}})$ *be the exact solutions to the coupled Stokes–Darcy flow problem* (13) *with homogeneous Dirichlet boundary conditions on the whole boundary (except the interface). Let* $(\mathbf{u}_h^{\mathcal{S}}, p_h^{\mathcal{S}}, p_h^{\mathcal{D}})$ *be the numerical solutions obtained from the finite element scheme* (40)*. Then for any* $\mathbf{v}_h \in \mathbf{V}_h^{\mathcal{S},0}$, $r_h \in W_h^{\mathcal{S},0}$, *and* $q_h \in V_h^{\mathcal{D},0}$, *there holds*

$$\begin{cases} \mathcal{A}_h^{\mathcal{S}}(\mathbf{e}_h^{\mathcal{S}}, \mathbf{v}_h) & -\mathcal{B}_h^{\mathcal{S}}(e_h^{\mathcal{S}}, \mathbf{v}_h) & +\mathcal{C}_h^{\mathcal{I}}(e_h^{\mathcal{D}}, \mathbf{v}_h) & = \mathcal{G}^{\mathcal{S}}(\mathbf{u}^{\mathcal{S}}, p^{\mathcal{S}}, p^{\mathcal{D}}, \mathbf{v}_h), \\ \mathcal{B}_h^{\mathcal{S}}(r_h, \mathbf{e}_h^{\mathcal{S}}) & & & = 0, \\ -\mathcal{C}_h^{\mathcal{I}}(q_h, \mathbf{e}_h^{\mathcal{S}}) & & +\mathcal{A}_h^{\mathcal{D}}(e_h^{\mathcal{D}}, q_h) & = \mathcal{G}^{\mathcal{D}}(\mathbf{u}^{\mathcal{D}}, q_h), \end{cases} \tag{52}$$

where

$$\begin{cases} \mathcal{G}^{\mathcal{S}}(\mathbf{u}^{\mathcal{S}}, p^{\mathcal{S}}, p^{\mathcal{D}}, \mathbf{v}_h) = \mathcal{A}_h^{\mathcal{S}}(\mathbf{P}_h \mathbf{u}^{\mathcal{S}} - \mathbf{u}^{\mathcal{S}}, \mathbf{v}_h) \\ \qquad -\mathcal{B}_h^{\mathcal{S}}(\pi_h p^{\mathcal{S}} - p^{\mathcal{S}}, \mathbf{v}_h) + \mathcal{C}_h^{\mathcal{I}}(Q_h p^{\mathcal{D}} - p^{\mathcal{D}}, \mathbf{v}_h), \\ \mathcal{G}^{\mathcal{D}}(\mathbf{u}^{\mathcal{D}}, q_h) = \sum_{E \in \mathcal{E}_h^{\mathcal{D}}} (\boldsymbol{\Pi}_h \mathbf{u}^{\mathcal{D}} - \mathbf{Q}_h \mathbf{u}^{\mathcal{D}}, \nabla_w q_h)_E. \end{cases} \tag{53}$$

Proof. To handle Darcy pressure error, we use the 3rd equation in the finite element scheme (40) to obtain

$$\begin{aligned} \mathcal{A}_h^{\mathcal{D}}(e_h^{\mathcal{D}}, q_h) &= \mathcal{A}_h^{\mathcal{D}}(Q_h p^{\mathcal{D}}, q_h) - \mathcal{A}_h^{\mathcal{D}}(p_h^{\mathcal{D}}, q_h) \\ &= \mathcal{A}_h^{\mathcal{D}}(Q_h p^{\mathcal{D}}, q_h) - \mathcal{F}_h^{\mathcal{D}}(q_h) - \mathcal{C}_h^{\mathcal{I}}(q_h, \mathbf{u}_h^{\mathcal{S}}). \end{aligned}$$

By Lemma 1, the first term in the last line is converted to

$$\begin{aligned} \mathcal{A}_h^{\mathcal{D}}(Q_h p^{\mathcal{D}}, q_h) &= \sum_{E \in \mathcal{E}_h^{\mathcal{D}}} (\mathbf{K} \nabla_w (Q_h p^{\mathcal{D}}), \nabla_w q_h)_E \\ &= \sum_{E \in \mathcal{E}_h^{\mathcal{D}}} (\mathbf{Q}_h (\mathbf{K} \nabla p^{\mathcal{D}}), \nabla_w q_h)_E \\ &= -\sum_{E \in \mathcal{E}_h^{\mathcal{D}}} (\mathbf{Q}_h \mathbf{u}^{\mathcal{D}}, \nabla_w q_h)_E. \end{aligned} \tag{54}$$

To deal with Darcy source term $s = \nabla \cdot (-\mathbf{K}\nabla p^{\mathcal{D}})$, we consider $q_h \in V_h^{\mathcal{D},0}$. Then

$$\begin{aligned}\mathcal{F}_h^{\mathcal{D}}(q_h) &= \sum_{E\in\mathcal{E}_h^{\mathcal{D}}} (s, q_h^{\circ})_{E^{\circ}} = \sum_{E\in\mathcal{E}_h^{\mathcal{D}}} \left(\nabla \cdot (-\mathbf{K}\nabla p^{\mathcal{D}}), q_h^{\circ}\right)_{E^{\circ}} \\ &= \sum_{E\in\mathcal{E}_h^{\mathcal{D}}} (\nabla \cdot \mathbf{u}^{\mathcal{D}}, q_h^{\circ})_{E^{\circ}} = \sum_{E\in\mathcal{E}_h^{\mathcal{D}}} (\nabla \cdot (\boldsymbol{\Pi}_h \mathbf{u}^{\mathcal{D}}), q_h^{\circ})_{E^{\circ}}.\end{aligned}$$

Note that $\boldsymbol{\Pi}_h \mathbf{u}^{\mathcal{D}}$ is in the global AC_0 space. By the definition of discrete weak gradient, we have

$$\mathcal{F}_h^{\mathcal{D}}(q_h) = \sum_{E\in\mathcal{E}_h^{\mathcal{D}}} \langle (\boldsymbol{\Pi}_h \mathbf{u}^{\mathcal{D}}) \cdot \mathbf{n}, q_h^{\partial}\rangle_{E^{\partial}} - \sum_{E\in\mathcal{E}_h^{\mathcal{D}}} (\boldsymbol{\Pi}_h \mathbf{u}^{\mathcal{D}}, \nabla_w q_h)_E.$$

The interpolant in the global AC_0 space has normal continuity. So the terms for the interior edges vanish, and the terms for Dirichlet edges satisfy $q_h^{\partial} = 0$. The only surviving terms lie on the interface edges. Thus we have

$$\mathcal{F}_h^{\mathcal{D}}(q_h) = \sum_{e\in\Gamma_h^{\mathcal{I}}} \langle (\boldsymbol{\Pi}_h \mathbf{u}^{\mathcal{D}}) \cdot \mathbf{n}^{\mathcal{D}}, q_h^{\partial}\rangle_e - \sum_{E\in\mathcal{E}_h^{\mathcal{D}}} (\boldsymbol{\Pi}_h \mathbf{u}^{\mathcal{D}}, \nabla_w q_h)_E. \tag{55}$$

Combining the above results yields

$$\begin{aligned}\mathcal{A}_h^{\mathcal{D}}(e_h^{\mathcal{D}}, q_h) = &\sum_{E\in\mathcal{E}_h^{\mathcal{D}}} (\boldsymbol{\Pi}_h \mathbf{u}^{\mathcal{D}} - \mathbf{Q}_h \mathbf{u}^{\mathcal{D}}, \nabla_w q_h)_E \\ &- \sum_{e\in\Gamma_h^{\mathcal{I}}} \langle (\boldsymbol{\Pi}_h \mathbf{u}^{\mathcal{D}}) \cdot \mathbf{n}^{\mathcal{D}}, q_h^{\partial}\rangle_e - C_h^{\mathcal{I}}(q_h, \mathbf{u}_h^{\mathcal{S}}).\end{aligned} \tag{56}$$

Therefore, subtracting $C_h^{\mathcal{I}}(q_h, \mathbf{e}_h^{\mathcal{S}})$ from $\mathcal{A}_h^{\mathcal{D}}(e_h^{\mathcal{D}}, q_h)$ yields

$$\begin{aligned}&\mathcal{A}_h^{\mathcal{D}}(e_h^{\mathcal{D}}, q_h) - C_h^{\mathcal{I}}(q_h, \mathbf{e}_h^{\mathcal{S}}) = \mathcal{A}_h^{\mathcal{D}}(e_h^{\mathcal{D}}, q_h) - C_h^{\mathcal{I}}(q_h, \mathbf{P}_h \mathbf{u}^{\mathcal{S}} - \mathbf{u}_h^{\mathcal{S}}) \\ &= \mathcal{A}_h^{\mathcal{D}}(e_h^{\mathcal{D}}, q_h) + C_h^{\mathcal{I}}(q_h, \mathbf{u}_h^{\mathcal{S}}) - C_h^{\mathcal{I}}(q_h, \mathbf{P}_h \mathbf{u}^{\mathcal{S}}) \\ &= \sum_{E\in\mathcal{E}_h^{\mathcal{D}}} (\boldsymbol{\Pi}_h \mathbf{u}^{\mathcal{D}} - \mathbf{Q}_h \mathbf{u}^{\mathcal{D}}, \nabla_w q_h)_E - \sum_{e\in\Gamma_h^{\mathcal{I}}} \langle (\boldsymbol{\Pi}_h \mathbf{u}^{\mathcal{D}}) \cdot \mathbf{n}^{\mathcal{D}}, q_h^{\partial}\rangle_e \\ &\quad - \sum_{e\in\Gamma_h^{\mathcal{I}}} \langle (\mathbf{P}_h \mathbf{u}^{\mathcal{S}}) \cdot \mathbf{n}^{\mathcal{S}}, q_h^{\partial}\rangle_e \\ &= \sum_{E\in\mathcal{E}_h^{\mathcal{D}}} (\boldsymbol{\Pi}_h \mathbf{u}^{\mathcal{D}} - \mathbf{Q}_h \mathbf{u}^{\mathcal{D}}, \nabla_w q_h)_E + \sum_{e\in\Gamma_h^{\mathcal{I}}} \langle (\mathbf{P}_h \mathbf{u}^{\mathcal{S}} - \boldsymbol{\Pi}_h \mathbf{u}^{\mathcal{D}}) \cdot \mathbf{n}^{\mathcal{D}}, q_h^{\partial}\rangle_e.\end{aligned} \tag{57}$$

By the flux-capturing property of the BR_1 interpolation operator (22), the flux capturing property of the AC_0 interpolation operator (31), and the first interface condition, the second sum vanishes, and one is led to the 3rd error equation in (52)

$$\begin{aligned}&\mathcal{A}_h^{\mathcal{D}}(e_h^{\mathcal{D}}, q_h) - C_h^{\mathcal{I}}(q_h, \mathbf{e}_h^{\mathcal{S}}) = \mathcal{A}_h^{\mathcal{D}}(e_h^{\mathcal{D}}, q_h) - C_h^{\mathcal{I}}(q_h, \mathbf{P}_h \mathbf{u}^{\mathcal{S}} - \mathbf{u}_h^{\mathcal{S}}) \\ &= \sum_{E\in\mathcal{E}_h^{\mathcal{D}}} (\boldsymbol{\Pi}_h \mathbf{u}^{\mathcal{D}} - \mathbf{Q}_h \mathbf{u}^{\mathcal{D}}, \nabla_w q_h)_E + \sum_{e\in\Gamma_h^{\mathcal{I}}} \langle (\mathbf{u}^{\mathcal{D}} - \boldsymbol{\Pi}_h \mathbf{u}^{\mathcal{D}}) \cdot \mathbf{n}^{\mathcal{D}}, q_h^{\partial}\rangle_e \\ &= \sum_{E\in\mathcal{E}_h^{\mathcal{D}}} (\boldsymbol{\Pi}_h \mathbf{u}^{\mathcal{D}} - \mathbf{Q}_h \mathbf{u}^{\mathcal{D}}, \nabla_w q_h)_E \\ &= \mathcal{G}^{\mathcal{D}}(\mathbf{u}^{\mathcal{D}}, q_h).\end{aligned} \tag{58}$$

To handle Stokes velocity error, we use the 1st equation in the finite element scheme (40). We remark that while the Stokes discretization is conforming, we proceed carefully due to the $\mathcal{C}_h^{\mathcal{I}}$ term to obtain

$$\begin{aligned}&\mathcal{A}_h^{\mathcal{S}}(\mathbf{e}_h^{\mathcal{S}}, \mathbf{v}_h) = \mathcal{A}_h^{\mathcal{S}}(\mathbf{P}_h \mathbf{u}^{\mathcal{S}}, \mathbf{v}_h) - \mathcal{A}_h^{\mathcal{S}}(\mathbf{u}_h^{\mathcal{S}}, \mathbf{v}_h) \\ &= \mathcal{A}_h^{\mathcal{S}}(\mathbf{P}_h \mathbf{u}^{\mathcal{S}}, \mathbf{v}_h) - \mathcal{F}_h^{\mathcal{S}}(\mathbf{v}_h) - \mathcal{B}_h^{\mathcal{S}}(p_h^{\mathcal{S}}, \mathbf{v}_h) + \mathcal{C}_h^{\mathcal{I}}(p_h^{\mathcal{D}}, \mathbf{v}_h).\end{aligned} \tag{59}$$

Similarly, we utilize Stokes 1st equation to rewrite the forcing term and obtain

$$\begin{aligned}\mathcal{F}_h^{\mathcal{S}}(\mathbf{v}_h) &= \sum_{E\in\mathcal{E}_h^{\mathcal{S}}}(\mathbf{f},\mathbf{v}_h)_E = \sum_{E\in\mathcal{E}_h^{\mathcal{S}}}(-\nabla\cdot\sigma,\mathbf{v}_h)_E\\ &= \sum_{E\in\mathcal{E}_h^{\mathcal{S}}}(\sigma,\nabla\mathbf{v}_h)_E - \langle\sigma\mathbf{n},\mathbf{v}_h\rangle_{E^\partial}\\ &= \sum_{E\in\mathcal{E}_h^{\mathcal{S}}}2\mu(\varepsilon(\mathbf{u}^{\mathcal{S}}),\varepsilon(\mathbf{v}_h))_E - (p^{\mathcal{S}},\nabla\cdot\mathbf{v}_h)_E - \langle\sigma\mathbf{n},\mathbf{v}_h\rangle_{E^\partial}.\end{aligned} \tag{60}$$

All normal contributions of stress cancel across the interior edges, leaving only the interface edges, where $\sigma\mathbf{n}^{\mathcal{S}}$ is once again decomposed into normal and tangential components, yielding

$$\begin{aligned}\mathcal{F}_h^{\mathcal{S}}(\mathbf{v}_h) &= \sum_{E\in\mathcal{E}_h^{\mathcal{S}}}2\mu(\varepsilon(\mathbf{u}^{\mathcal{S}}),\varepsilon(\mathbf{v}_h))_E - (p^{\mathcal{S}},\nabla\cdot\mathbf{v}_h)_E\\ &\quad+\sum_{e\in\mathcal{E}_h^{\mathcal{I}}}\langle\beta\mathbf{u}^{\mathcal{S}}\cdot\mathbf{t}^{\mathcal{S}},\mathbf{v}_h\cdot\mathbf{t}^{\mathcal{S}}\rangle_e + \langle p^{\mathcal{D}},\mathbf{v}_h\cdot\mathbf{n}^{\mathcal{S}}\rangle_e.\end{aligned} \tag{61}$$

So we have

$$\begin{aligned}\mathcal{F}_h^{\mathcal{S}}(\mathbf{v}_h) &= \sum_{E\in\mathcal{E}_h^{\mathcal{S}}}2\mu(\varepsilon(\mathbf{u}^{\mathcal{S}}),\varepsilon(\mathbf{v}_h))_E + \sum_{e\in\mathcal{E}_h^{\mathcal{I}}}\langle\beta\mathbf{u}^{\mathcal{S}}\cdot\mathbf{t}^{\mathcal{S}},\mathbf{v}_h\cdot\mathbf{t}^{\mathcal{S}}\rangle_e\\ &\quad-\mathcal{B}_h^{\mathcal{S}}(p^{\mathcal{S}},\mathbf{v}_h)+\mathcal{C}_h^{\mathcal{I}}(p^{\mathcal{D}},\mathbf{v}_h).\end{aligned} \tag{62}$$

Therefore,

$$\begin{aligned}\mathcal{A}_h^{\mathcal{S}}(\mathbf{e}_h^{\mathcal{S}},\mathbf{v}_h) &= \mathcal{A}_h^{\mathcal{S}}(\mathbf{P}_h\mathbf{u}^{\mathcal{S}},\mathbf{v}_h) - \sum_{E\in\mathcal{E}_h^{\mathcal{S}}}2\mu(\varepsilon(\mathbf{u}^{\mathcal{S}}),\varepsilon(\mathbf{v}_h))_E\\ &\quad-\sum_{e\in\mathcal{E}_h^{\mathcal{I}}}\langle\beta\mathbf{u}^{\mathcal{S}}\cdot\mathbf{t}^{\mathcal{S}},\mathbf{v}_h\cdot\mathbf{t}^{\mathcal{S}}\rangle_e + \mathcal{B}_h^{\mathcal{S}}(p^{\mathcal{S}}-p_h^{\mathcal{S}},\mathbf{v}_h) - \mathcal{C}_h^{\mathcal{I}}(p^{\mathcal{D}}-p_h^{\mathcal{D}},\mathbf{v}_h)\\ &= \mathcal{A}_h^{\mathcal{S}}(\mathbf{P}_h\mathbf{u}^{\mathcal{S}}-\mathbf{u}^{\mathcal{S}},\mathbf{v}_h) + \mathcal{B}_h^{\mathcal{S}}(p^{\mathcal{S}}-\pi_h p^{\mathcal{S}}+\pi_h p^{\mathcal{S}}-p_h^{\mathcal{S}},\mathbf{v}_h)\\ &\quad-\mathcal{C}_h^{\mathcal{I}}(p^{\mathcal{D}}-Q_h p^{\mathcal{D}}+Q_h p^{\mathcal{D}}-p_h^{\mathcal{D}},\mathbf{v}_h)\\ &= \mathcal{A}_h^{\mathcal{S}}(\mathbf{P}_h\mathbf{u}^{\mathcal{S}}-\mathbf{u}^{\mathcal{S}},\mathbf{v}_h) + \mathcal{B}_h^{\mathcal{S}}(e_h^{\mathcal{S}},\mathbf{v}_h) - \mathcal{C}_h^{\mathcal{I}}(e_h^{\mathcal{D}},\mathbf{v}_h)\\ &\quad-\mathcal{B}_h^{\mathcal{S}}(\pi_h p^{\mathcal{S}}-p^{\mathcal{S}},\mathbf{v}_h)+\mathcal{C}_h^{\mathcal{I}}(Q_h p^{\mathcal{D}}-p^{\mathcal{D}},\mathbf{v}_h)\\ &= \mathcal{G}^{\mathcal{S}}(\mathbf{u}^{\mathcal{S}},p^{\mathcal{S}},p^{\mathcal{D}},\mathbf{v}_h) + \mathcal{B}_h^{\mathcal{S}}(e_h^{\mathcal{S}},\mathbf{v}_h) - \mathcal{C}_h^{\mathcal{I}}(e_h^{\mathcal{D}},\mathbf{v}_h),\end{aligned} \tag{63}$$

which yields the 1st error equation in (52).

6.4. Error estimation

For the approximation capacity of the finite element spaces used for the scheme in this paper, one has the following results. For any quadrilateral element E, there holds

$$\begin{aligned}&\|\mathbf{u}^{\mathcal{S}}-\mathbf{P}_h\mathbf{u}^{\mathcal{S}}\|_k \lesssim h^{2-k}\|\mathbf{u}^{\mathcal{S}}\|_{\mathbf{H}^2(E)}, \quad k=0,1;\\ &\|p^{\mathcal{S}}-\pi_h p^{\mathcal{S}}\|_0 \lesssim h\|p^{\mathcal{S}}\|_{H^1(E)}.\end{aligned} \tag{64}$$

Additionally, we shall frequently use the following standard trace inequality for any scalar- or vector-valued H^1-function

$$h_E\|\phi\|_e^2 \lesssim \|\phi\|_0^2 + h_E^2|\phi|_1^2. \tag{65}$$

Based on these facts, we have

$$\|(\mathbf{u}^{\mathcal{S}}-\mathbf{P}_h\mathbf{u}^{\mathcal{S}})\cdot\mathbf{t}\|_e \lesssim h_E^{\frac{3}{2}}\|\mathbf{u}^{\mathcal{S}}\|_{\mathbf{H}^2(E)}. \tag{66}$$

We shall also use the following bounds for norms of a function $\mathbf{v} \in \mathbf{H}^1(\Omega^{\mathcal{S}})$:

$$\|\nabla \cdot \mathbf{v}\|_{L^2(\Omega^{\mathcal{S}})} \lesssim \|\varepsilon(\mathbf{v})\|_{\mathbf{L}^2(\Omega^{\mathcal{S}})} \leq \|\nabla \mathbf{v}\|_{\mathbf{L}^2(\Omega^{\mathcal{S}})} \leq \|\mathbf{v}\|_{\mathbf{H}^1(\Omega^{\mathcal{S}})}. \tag{67}$$

Theorem 1 (*Energy Norm Error Estimate*)**.** *Let* $(\mathbf{u}^{\mathcal{S}}, p^{\mathcal{S}}, p^{\mathcal{D}}) \in \mathbf{H}^2(\Omega^{\mathcal{S}}) \times H^1(\Omega^{\mathcal{S}}) \times H^2(\Omega^{\mathcal{D}})$ *be the full-regularity solutions to (1–5) under the assumptions from the beginning of this section. Let* $(\mathbf{u}_h^{\mathcal{S}}, p_h^{\mathcal{S}}, p_h^{\mathcal{D}}) \in \mathbf{V}_h^{\mathcal{S},0} \times W_h^{\mathcal{S}} \times V_h^{\mathcal{D},0}$ *be the numerical solutions of* (40)*. Then*

$$\begin{aligned} |\!|\!|(\mathbf{e}_h^{\mathcal{S}}, e_h^{\mathcal{D}})|\!|\!|_h &\lesssim h\left(\|\mathbf{u}^{\mathcal{S}}\|_{\mathbf{H}^2(\Omega^{\mathcal{S}})} + \|p^{\mathcal{S}}\|_{H^1(\Omega^{\mathcal{S}})} + \|p^{\mathcal{D}}\|_{H^2(\Omega^{\mathcal{D}})}\right), \\ \|e_h^{\mathcal{S}}\| &\lesssim h\left(\|\mathbf{u}^{\mathcal{S}}\|_{\mathbf{H}^2(\Omega^{\mathcal{S}})} + \|p^{\mathcal{S}}\|_{H^1(\Omega^{\mathcal{S}})} + \|p^{\mathcal{D}}\|_{H^2(\Omega^{\mathcal{D}})}\right). \end{aligned} \tag{68}$$

Proof. Taking $\mathbf{v}_h = \mathbf{e}_h^{\mathcal{S}}$, $r_h = e_h^{\mathcal{S}}$, and $q_h = e_h^{\mathcal{D}}$ in the error equations (52) and summing them yields

$$\begin{aligned} |\!|\!|(\mathbf{e}_h^{\mathcal{S}}, e_h^{\mathcal{D}})|\!|\!|_h^2 &= |\!|\!|\mathbf{e}_h^{\mathcal{S}}|\!|\!|_h^2 + |\!|\!|e_h^{\mathcal{D}}|\!|\!|_h^2 = \mathcal{A}_h^{\mathcal{S}}(\mathbf{e}_h^{\mathcal{S}}, \mathbf{e}_h^{\mathcal{S}}) + \mathcal{A}_h^{\mathcal{D}}(e_h^{\mathcal{D}}, e_h^{\mathcal{D}}) \\ &= \mathcal{G}^{\mathcal{S}}(\mathbf{u}^{\mathcal{S}}, p^{\mathcal{S}}, p^{\mathcal{D}}, \mathbf{e}_h^{\mathcal{S}}) + \mathcal{G}^{\mathcal{D}}(\mathbf{u}^{\mathcal{D}}, e_h^{\mathcal{D}}). \end{aligned} \tag{69}$$

Part (1) Handling $\mathcal{G}^{\mathcal{S}}(\mathbf{u}^{\mathcal{S}}, p^{\mathcal{S}}, p^{\mathcal{D}}, \mathbf{e}_h^{\mathcal{S}})$. Recall that

$$\mathcal{G}^{\mathcal{S}}(\mathbf{u}^{\mathcal{S}}, p^{\mathcal{S}}, p^{\mathcal{D}}, \mathbf{v}_h) = \mathcal{A}_h^{\mathcal{S}}(\mathbf{P}_h\mathbf{u}^{\mathcal{S}} - \mathbf{u}^{\mathcal{S}}, \mathbf{v}_h) - \mathcal{B}_h^{\mathcal{S}}(\pi_h p^{\mathcal{S}} - p^{\mathcal{S}}, \mathbf{v}_h) + \mathcal{C}_h^{\mathcal{I}}(Q_h p^{\mathcal{D}} - p^{\mathcal{D}}, \mathbf{v}_h).$$

The three terms on the right-hand side of $\mathcal{G}^{\mathcal{S}}$ will be estimated individually.

(i) For $\mathcal{A}_h^{\mathcal{S}}(\mathbf{P}_h\mathbf{u}^{\mathcal{S}} - \mathbf{u}^{\mathcal{S}}, \mathbf{e}_h)$, by applying triangle inequalities, Cauchy–Schwarz inequalities, trace inequalities, and the following fact that is derived from (67):

$$\|\varepsilon(\mathbf{P}_h\mathbf{u}^{\mathcal{S}} - \mathbf{u}^{\mathcal{S}})\|_{\mathbf{L}^2(\Omega^{\mathcal{S}})} \lesssim \|\mathbf{P}_h\mathbf{u}^{\mathcal{S}} - \mathbf{u}^{\mathcal{S}}\|_{\mathbf{H}^1(\Omega^{\mathcal{S}})},$$

we obtain

$$\begin{aligned} &\left|\mathcal{A}_h^{\mathcal{S}}(\mathbf{P}_h\mathbf{u}^{\mathcal{S}} - \mathbf{u}^{\mathcal{S}}, \mathbf{e}_h^{\mathcal{S}})\right| \\ &= \left|\sum_{E\in\mathcal{E}_h^{\mathcal{S}}} 2\mu(\varepsilon(\mathbf{P}_h\mathbf{u}^{\mathcal{S}} - \mathbf{u}^{\mathcal{S}}), \varepsilon(\mathbf{e}_h^{\mathcal{S}}))_E + \sum_{e\in\mathcal{E}_h^{\mathcal{I}}} \langle\beta(\mathbf{P}_h\mathbf{u}^{\mathcal{S}} - \mathbf{u}^{\mathcal{S}})\cdot\mathbf{t}^{\mathcal{S}}, \mathbf{e}_h^{\mathcal{S}}\cdot\mathbf{t}^{\mathcal{S}}\rangle_e\right| \\ &\leq 2\mu\left(\sum_{E\in\mathcal{E}_h^{\mathcal{S}}} \|\varepsilon(\mathbf{P}_h\mathbf{u}^{\mathcal{S}} - \mathbf{u}^{\mathcal{S}})\|_E^2\right)^{\frac{1}{2}}\left(\sum_{E\in\mathcal{E}_h^{\mathcal{S}}} \|\varepsilon(\mathbf{e}_h^{\mathcal{S}})\|_E^2\right)^{\frac{1}{2}} \\ &\quad + \left(\sum_{e\in\mathcal{E}_h^{\mathcal{I}}} \|(\mathbf{P}_h\mathbf{u}^{\mathcal{S}} - \mathbf{u}^{\mathcal{S}})\cdot\mathbf{t}^{\mathcal{S}}\|_e^2\right)^{\frac{1}{2}}\left(\sum_{e\in\mathcal{E}_h^{\mathcal{I}}} \|\beta^{\frac{1}{2}}\mathbf{e}_h^{\mathcal{S}}\cdot\mathbf{t}^{\mathcal{S}}\|_e^2\right)^{\frac{1}{2}} \\ &\lesssim h\|\mathbf{u}^{\mathcal{S}}\|_{\mathbf{H}^2(\Omega^{\mathcal{S}})}|\!|\!|\mathbf{e}_h^{\mathcal{S}}|\!|\!|_h + h^{\frac{3}{2}}\|\mathbf{u}^{\mathcal{S}}\|_{\mathbf{H}^2(\Omega^{\mathcal{S}})}|\!|\!|\mathbf{e}_h^{\mathcal{S}}|\!|\!|_h. \end{aligned} \tag{70}$$

For $\mathcal{B}_h^{\mathcal{S}}(p^{\mathcal{S}} - \pi_h p^{\mathcal{S}}, \mathbf{e}_h^{\mathcal{S}})$, we apply similar techniques to obtain

$$\begin{aligned} \left|\mathcal{B}_h^{\mathcal{S}}(p^{\mathcal{S}} - \pi_h p^{\mathcal{S}}, \mathbf{e}_h^{\mathcal{S}})\right| &= \left|\sum_{E\in\mathcal{E}_h^{\mathcal{S}}} (p^{\mathcal{S}} - \pi_h p^{\mathcal{S}}, \nabla\cdot\mathbf{e}_h^{\mathcal{S}})_E\right| \\ &\leq \left(\sum_{E\in\mathcal{E}_h^{\mathcal{S}}} \|p^{\mathcal{S}} - \pi_h p^{\mathcal{S}}\|_E^2\right)^{\frac{1}{2}}\left(\sum_{E\in\mathcal{E}_h^{\mathcal{S}}} \|\nabla\cdot\mathbf{e}_h^{\mathcal{S}}\|_E^2\right)^{\frac{1}{2}} \\ &\leq \|p^{\mathcal{S}} - \pi_h p^{\mathcal{S}}\|_{L^2(\Omega^{\mathcal{S}})}\|\nabla\cdot\mathbf{e}_h^{\mathcal{S}}\|_{L^2(\Omega^{\mathcal{S}})} \\ &\lesssim h\|p^{\mathcal{S}}\|_{H^1(\Omega^{\mathcal{S}})}\|\varepsilon(\mathbf{e}_h^{\mathcal{S}})\|_{L^2(\Omega^{\mathcal{S}})} \\ &\leq h\|p^{\mathcal{S}}\|_{H^1(\Omega^{\mathcal{S}})}|\!|\!|\mathbf{e}_h^{\mathcal{S}}|\!|\!|_h. \end{aligned} \tag{71}$$

Finally, for $\mathcal{C}_h^{\mathcal{I}}(p^{\mathcal{D}} - Q_h p^{\mathcal{D}}, \mathbf{e}_h^{\mathcal{S}})$, we estimate its interface terms by using the techniques for duality pairing in [35]. This yields

$$\begin{aligned}\left|\mathcal{C}_h^{\mathcal{I}}(p^{\mathcal{D}} - Q_h p^{\mathcal{D}}, \mathbf{e}_h^{\mathcal{S}})\right| &= \left|\sum_{e\in\mathcal{E}_h^{\mathcal{I}}} \langle p^{\mathcal{D}} - Q_h p^{\mathcal{D}}, \mathbf{e}_h^{\mathcal{S}}\cdot\mathbf{n}\rangle_e\right| \\ &\le \|p^{\mathcal{D}} - Q_h p^{\mathcal{D}}\|_{H^{-\frac{1}{2}}(\Gamma_h^{\mathcal{I}})} \|\mathbf{e}_h^{\mathcal{S}}\cdot\mathbf{n}\|_{H^{\frac{1}{2}}(\Gamma_h^{\mathcal{I}})} \\ &\le h\|p^{\mathcal{D}}\|_{H^{\frac{1}{2}}(\Gamma^{\mathcal{I}})} \|\mathbf{e}_h^{\mathcal{S}}\|_{\mathbf{H}^1(\Omega_h^{\mathcal{S}})} \\ &\le h\|p^{\mathcal{D}}\|_{H^1(\Omega^{\mathcal{D}})} |\|\mathbf{e}_h^{\mathcal{S}}\||_h,\end{aligned} \tag{72}$$

where the inequalities for $\mathbf{e}_h^{\mathcal{S}}$ are due to a trace inequality and then the Korn's inequality.

Part (2) Handling $\mathcal{G}^{\mathcal{D}}(\mathbf{u}^{\mathcal{D}}, e_h^{\mathcal{D}})$. Recall that

$$\mathcal{G}^{\mathcal{D}}(\mathbf{u}^{\mathcal{D}}, q_h) = \sum_{E\in\mathcal{E}_h^{\mathcal{D}}} (\boldsymbol{\Pi}_h\mathbf{u}^{\mathcal{D}} - \mathbf{Q}_h\mathbf{u}^{\mathcal{D}}, \nabla_w q_h)_E.$$

This involves two approximations to $\mathbf{u}^{\mathcal{D}}$. Each converges with first order. Based on the approximation capacity of $\boldsymbol{\Pi}_h, \mathbf{Q}_h$ (and triangle inequalities), we have, for each element E,

$$\|\boldsymbol{\Pi}_h\mathbf{u}^{\mathcal{D}} - \mathbf{Q}_h\mathbf{u}^{\mathcal{D}}\|_E \le \|\boldsymbol{\Pi}_h\mathbf{u}^{\mathcal{D}} - \mathbf{u}^{\mathcal{D}}\|_E + \|\mathbf{u}^{\mathcal{D}} - \mathbf{Q}_h\mathbf{u}^{\mathcal{D}}\|_E \lesssim h\|\mathbf{u}^{\mathcal{D}}\|_{\mathbf{H}^1(E)}.$$

Then by the Cauchy–Schwarz inequality, we have

$$\begin{aligned}\mathcal{G}^{\mathcal{D}}(\mathbf{u}^{\mathcal{D}}, e_h^{\mathcal{D}}) &= \sum_{E\in\mathcal{E}_h^{\mathcal{D}}} (\boldsymbol{\Pi}_h\mathbf{u}^{\mathcal{D}} - \mathbf{Q}_h\mathbf{u}^{\mathcal{D}}, \nabla_w e_h^{\mathcal{D}})_E \\ &\le \left(\sum_{E\in\mathcal{E}_h^{\mathcal{D}}} \|\boldsymbol{\Pi}_h\mathbf{u}^{\mathcal{D}} - \mathbf{Q}_h\mathbf{u}^{\mathcal{D}}\|_E^2\right)^{\frac{1}{2}} \left(\sum_{E\in\mathcal{E}_h^{\mathcal{D}}} \|\nabla_w e_h^{\mathcal{D}}\|_E^2\right)^{\frac{1}{2}} \\ &\lesssim h\|\mathbf{u}^{\mathcal{D}}\|_{\mathbf{H}^1(\Omega^{\mathcal{D}})} \frac{1}{\sqrt{\kappa}} |\|e_h^{\mathcal{D}}\||_h,\end{aligned} \tag{73}$$

where in the last step we have used the fact $|\|e_h^{\mathcal{D}}\||_h^2 \ge \kappa \sum_{E\in\mathcal{E}_h^{\mathcal{D}}} \|\nabla_w e_h^{\mathcal{D}}\|_E^2$.

Combining these results, noting that $\|\mathbf{u}^{\mathcal{D}}\|_1 \lesssim \|p^{\mathcal{D}}\|_2$ and dividing both sides by $|\|(\mathbf{e}_h^{\mathcal{S}}, e_h^{\mathcal{D}})\||_h$ yields the first inequality in (68).

Part (3) Handling $\|e_h^{\mathcal{S}}\|$. First, we remark that solving the first error equation (52) for $\mathcal{B}_h^{\mathcal{S}}$ yields

$$\left|\mathcal{B}_h^{\mathcal{S}}(e_h^{\mathcal{S}}, \mathbf{v}_h)\right| = \left|\mathcal{A}_h^{\mathcal{S}}(\mathbf{e}_h^{\mathcal{S}}, \mathbf{v}_h) + \mathcal{C}_h^{\mathcal{I}}(e_h^{\mathcal{D}}, \mathbf{v}_h) - \mathcal{G}^{\mathcal{S}}(\mathbf{u}^{\mathcal{S}}, p^{\mathcal{S}}, p^{\mathcal{D}}, \mathbf{v}_h)\right|.$$

This holds true for each $\mathbf{v}_h \in \mathbf{V}_h^{\mathcal{S},0}$, so we may additionally restrict $\mathbf{v}|_{\Gamma^{\mathcal{I}}} \equiv 0$, for which we denote by $\mathbf{v} \in \mathbf{V}_h^0 \subset \mathbf{V}_h^{\mathcal{S},0}$ to obtain

$$\begin{aligned}&\left|\mathcal{B}_h^{\mathcal{S}}(e_h^{\mathcal{S}}, \mathbf{v}_h)\right| = \left|\mathcal{A}_h^{\mathcal{S}}(\mathbf{e}_h^{\mathcal{S}}, \mathbf{v}_h) - \mathcal{G}^{\mathcal{S}}(\mathbf{u}^{\mathcal{S}}, p^{\mathcal{S}}, p^{\mathcal{D}}, \mathbf{v}_h)\right| \\ &\lesssim |\|\mathbf{e}_h^{\mathcal{S}}\||_h |\|\mathbf{v}_h\||_h + h\left(\|\mathbf{u}^{\mathcal{S}}\|_{\mathbf{H}^2(\Omega^{\mathcal{S}})} + \|p^{\mathcal{S}}\|_{H^1(\Omega^{\mathcal{S}})} + \|p^{\mathcal{D}}\|_{H^2(\Omega^{\mathcal{D}})}\right) |\|\mathbf{v}_h\||_h \\ &\lesssim h\left(\|\mathbf{u}^{\mathcal{S}}\|_{\mathbf{H}^2(\Omega^{\mathcal{S}})} + \|p^{\mathcal{S}}\|_{H^1(\Omega^{\mathcal{S}})} + \|p^{\mathcal{D}}\|_{H^2(\Omega^{\mathcal{D}})}\right) |\|\mathbf{v}_h\||_h.\end{aligned} \tag{74}$$

The inf–sup condition for $\mathcal{B}_h^{\mathcal{S}}$ is well-known in the case of Stokes flow [27], and it applies to $\mathbf{v}_h \in \mathbf{V}_h^0$. Therefore, we have

$$\begin{aligned}\|e_h^{\mathcal{S}}\|_{L^2(\Omega^{\mathcal{S}})} &\lesssim \sup_{\mathbf{v}\in\mathbf{V}_h^0} \frac{|\mathcal{B}_h^{\mathcal{S}}(e_h^{\mathcal{S}}, \mathbf{v}_h)|}{|\|\mathbf{v}_h\||_h} \\ &\lesssim h\left(\|\mathbf{u}^{\mathcal{S}}\|_{\mathbf{H}^2(\Omega^{\mathcal{S}})} + \|p^{\mathcal{S}}\|_{H^1(\Omega^{\mathcal{S}})} + \|p^{\mathcal{D}}\|_{H^2(\Omega^{\mathcal{D}})}\right),\end{aligned} \tag{75}$$

which concludes the proof.

Table 1
Example 1: Errors and convergence rates.

n	$\|\|\|(\mathbf{e}_h^{\mathcal{S}}, e_h^{\mathcal{D}})\|\|\|_h$	Rate	$\|\mathbf{u}^{\mathcal{S}} - \mathbf{u}_h^{\mathcal{S}}\|_{L^2}$	Rate	$\|p^{\mathcal{S}} - p_h^{\mathcal{S}}\|_{L^2}$	Rate	$\|p^{\mathcal{D}} - p_h^{\mathcal{D}}\|_{L^2}$	Rate
8	7.8259e−01	–	1.2155e−02	–	1.0935e−01	–	2.7940e−01	–
16	4.0407e−01	0.95	2.7537e−03	2.14	5.3808e−02	1.02	1.4024e−01	0.99
32	2.0363e−01	0.98	6.6788e−04	2.04	2.6794e−02	1.00	7.0189e−02	0.99
64	1.0201e−01	0.99	1.6564e−04	2.01	1.3383e−02	1.00	3.5103e−02	0.99
128	5.1031e−02	0.99	4.1328e−05	2.00	6.6898e−03	1.00	1.7553e−02	0.99

Remarks. In addition to the results proved above, we expect first-order convergence of Darcy velocity in the $H(\mathrm{div})$-norm. Although it is not formally proved here, rigorous analysis for the case of single-phase Darcy flow only can be found in [28]. We anticipate a similar result for the Stokes–Darcy problem, provided the Stokes solution to which the Darcy solution is coupled converges at an appropriate rate. We provide numerical support for our claim in Example 2 in Section 7.

In addition to the $H(\mathrm{div})$-convergence discussed above, our numerical experiments in the following section suggest

- L^2-norm of Stokes velocity errors exhibits 2nd order convergence;
- L^2-norm of Darcy pressure errors exhibits 1st order convergence.

7. Numerical experiments

This section presents numerical experiments to demonstrate accuracy and efficiency of our new finite element solver for coupled Stokes–Darcy flow problems.

Example 1 (*Known Analytical Solutions*)**.** First we consider an example that has known analytical solutions. The example is taken from [22]. Specifically, the domain for Stokes flow is $\Omega^{\mathcal{S}} = (0, \pi) \times (0, 1)$, the domain for Darcy flow is $\Omega^{\mathcal{D}} = (0, \pi) \times (-1, 0)$, and the interface is $\Gamma^{\mathcal{I}} = (0, \pi) \times \{y = 0\}$. Fluid viscosity is set as $\mu = 1$, the permeability matrix is $\mathbf{K} = \mathbf{I}$, and $\mathbf{f}^{\mathcal{D}} = \mathbf{0}$.

For the Stokes part, the exact solutions for velocity and pressure are

$$\mathbf{u}^{\mathcal{S}}(x, y) = \begin{bmatrix} \cos(x)v'(y) \\ \sin(x)v(y) \end{bmatrix}, \qquad p^{\mathcal{S}}(x, y) = \sin(x)\sin(y),$$

where $v(y) = \frac{1}{\pi^2}\sin^2(\pi y) - 2$. Clearly, $\nabla \cdot \mathbf{u}^{\mathcal{S}} = 0$. For the Darcy part, one has

$$p^{\mathcal{D}}(x, y) = \sin(x)(e^y - e^{-y}), \qquad \mathbf{u}^{\mathcal{D}}(x, y) = -\begin{bmatrix} \cos(x)(e^y - e^{-y}) \\ \sin(x)(e^y + e^{-y}) \end{bmatrix}.$$

The BJS coefficient $\alpha = 1$. The three interface conditions can be easily verified.

Example 1 is tested on a sequence of uniform rectangular meshes that have n partitions in each of x, y-directions. In this case, the local AC_0 space is the same as the classical $RT_{[0]}$ space. The numerical results in Table 1 demonstrate the proved first order convergence in the discrete error energy norm, in addition to the Stokes pressure error L^2-norm. We remark that although it was not proved, for this numerical example, we observe second order convergence in the Stokes velocity error L^2-norm and first order convergence in the Darcy pressure error L^2-norm.

Example 2 (*Trapezoidal Meshes and $H(div)$-Approximation*)**.** This example demonstrates that our new solver applies well to general convex quadrilateral meshes, as shown in Fig. 2. We observe optimal order $H(\mathrm{div})$-approximation in Darcy velocity since the new Arbogast–Correa space is used. This example is adopted from the one in [4] on p. 383 with a slight modification in the Stokes velocity to ensure that the BJS condition is satisfied with non-zero data.

Specifically, $\Omega^{\mathcal{S}} = (0, 1) \times (1, 2)$, $\Omega^{\mathcal{D}} = (0, 1) \times (0, 1)$, the interface is $\Gamma^{\mathcal{I}} = (0, 1) \times \{y = 1\}$. For Darcy flow, the permeability matrix is $\mathbf{K} = \kappa\mathbf{I}$ with $\kappa = 1$. In addition, $\mathbf{f}^{\mathcal{D}} = \mathbf{0}$. An exact solution for the pressure is given as

$$p^{\mathcal{D}}(x, y) = \frac{2}{\pi}\cos\left(\frac{\pi}{2}x\right)\cos\left(\frac{\pi}{2}y\right) + (1 - x)y, \tag{76}$$

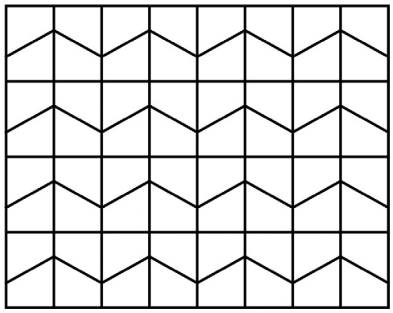

Fig. 2. Example 2: A trapezoidal mesh with a slant parameter 0.35. See [36] also.

Table 2
Example 2: Convergence rates of CG(BR_1, Q_0) + WG(P_0, P_0; AC_0) solver on trapezoidal meshes with slant parameter 0.35.

n	$\|\mathbf{u}^{\mathcal{S}} - \mathbf{u}_h^{\mathcal{S}}\|_{\mathbf{L}^2}$	Rate	$\|p^{\mathcal{D}} - p_h^{\mathcal{D}}\|_{L^2}$	Rate	$\|\mathbf{u}^{\mathcal{D}} - \mathbf{u}_h^{\mathcal{D}}\|_{\mathbf{L}^2}$	Rate	$\|\nabla\cdot(\mathbf{u}^{\mathcal{D}} - \mathbf{u}_h^{\mathcal{D}})\|_{L^2}$	Rate
2^3	7.8401e−03	–	3.8603e−02	–	6.4434e−02	–	2.1566e−01	–
2^4	2.0155e−03	1.95	1.9485e−02	0.98	3.2998e−02	0.96	1.0819e−01	0.99
2^5	5.1152e−04	1.97	9.7684e−03	0.99	1.6644e−02	0.98	5.4139e−02	0.99
2^6	1.2908e−04	1.98	4.8884e−03	0.99	8.3532e−03	0.99	2.7075e−02	0.99
2^7	3.2461e−05	1.99	2.4450e−03	0.99	4.1838e−03	0.99	1.3538e−02	0.99

which produces a Darcy velocity

$$\mathbf{u}^{\mathcal{D}}(x,y) = \begin{bmatrix} \sin\left(\frac{\pi}{2}x\right)\cos\left(\frac{\pi}{2}y\right) + y \\ \cos\left(\frac{\pi}{2}x\right)\sin\left(\frac{\pi}{2}y\right) - (1-x) \end{bmatrix}, \tag{77}$$

and accordingly, the fluid source is

$$s(x,y) = \pi\cos\left(\frac{\pi}{2}x\right)\cos\left(\frac{\pi}{2}y\right). \tag{78}$$

We use the above $p^{\mathcal{D}}, \mathbf{u}^{\mathcal{D}}$ to specify a Dirichlet boundary condition on the bottom side and a Neumann boundary condition on the lateral sides. For Stokes flow, we have $\mu = 1$. The exact solutions for velocity and pressure are known as

$$\mathbf{u}^{\mathcal{S}} = \begin{bmatrix} 1 - \sin\left(\frac{\pi}{2}x\right)\cos\left(\frac{\pi}{2}y\right) \\ -(1-x) + \cos\left(\frac{\pi}{2}x\right)\sin\left(\frac{\pi}{2}y\right) \end{bmatrix}, \qquad p^{\mathcal{S}} = 1 - x. \tag{79}$$

The body force $\mathbf{f}^{\mathcal{S}}$ is derived accordingly. Clearly, $\nabla\cdot\mathbf{u}^{\mathcal{S}} = 0$. The velocity exact solution is used to pose Dirichlet boundary conditions on the left and right-sides of $\Omega^{\mathcal{S}}$. A Neumann condition is posed on the top side. The BJS constant $\alpha = 1$. It can be verified that all three interface conditions are satisfied.

For numerical experiments, we use a family of trapezoidal meshes (with a slant parameter 0.35) as shown in Fig. 2. This type of meshes was introduced in [36]. Table 2 shows the results obtained from using the new solver developed in this paper. One can clearly observe 2nd order convergence in Stokes velocity and 1st order convergence in Darcy pressure, velocity, and div of velocity. However, Table 3 exhibits no convergence at all when the unmapped Raviart–Thomas space is used on trapezoidal meshes.

Example 3 (*Lid-Driven Cavity + Heterogeneous Permeability*)**.** This example couples the well-known lid-driven cavity problem for Stokes flow and Darcy flow in a heterogeneous permeability field. Here the Stokes domain is $\Omega^{\mathcal{S}} = (0,2)\times(0,1)$ whereas the Darcy domain is $\Omega^{\mathcal{D}} = (0,2)\times(-1,0)$.

For the Stokes part, $\mu = 1$. There is no body force. Dirichlet boundary conditions are posed. Specifically, for the top-side ($y = 1$), one has $\mathbf{u}_D^{\mathcal{S}} = [1,0]^T$; for the left- and right-sides, a no-slip boundary condition ($\mathbf{u} = \mathbf{0}$) is posed.

Table 3
Example 2: **No convergence** for the combination of CG(BR_1, Q_0) and WG(Q_0, Q_0; $RT_{[0]}$) on trapezoidal meshes with a slant parameter 0.35.

n	$\|\mathbf{u}^{\mathcal{S}} - \mathbf{u}_h^{\mathcal{S}}\|_{\mathbf{L}^2}$	$\|p^{\mathcal{D}} - p_h^{\mathcal{D}}\|_{L^2}$	$\|\mathbf{u}^{\mathcal{D}} - \mathbf{u}_h^{\mathcal{D}}\|_{\mathbf{L}^2}$	$\|\nabla\cdot(\mathbf{u}^{\mathcal{D}} - \mathbf{u}_h^{\mathcal{D}})\|_{L^2}$
2^3	7.9157e−03	3.9068e−02	1.4909e−01	2.8331e+00
2^4	2.0827e−03	2.0143e−02	1.4671e−01	6.2122e+00
2^5	6.0593e−04	1.1058e−02	1.4924e−01	1.3150e+01
2^6	2.8866e−04	7.2183e−03	1.5137e−01	2.7046e+01
2^7	2.4347e−04	5.9187e−03	1.5264e−01	5.4833e+01

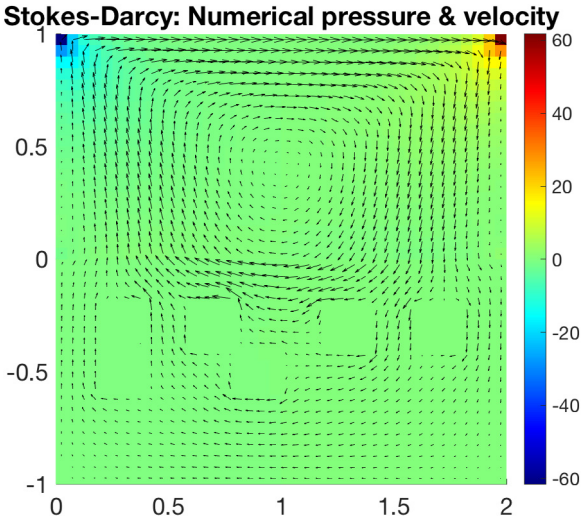

Fig. 3. Example 3: Numerical velocity and pressure obtained from using CG(BR_1, Q_0) + WG(P_0, P_0; AC_0) on a rectangular mesh with $h = 1/20$. Velocity is plotted at element centers and the magnitude is doubled for better visual effect.

For the Darcy part, a heterogeneous permeability $\mathbf{K} = \kappa\mathbf{I}$ is given. Specifically, $\Omega^{\mathcal{D}}$ is divided uniformly into 10×5 blocks. Labeling from left to right and top to bottom, these six blocks have a very low permeability value $\kappa = 10^{-6}$: $(2, 2), (2, 4), (2, 7), (2, 9), (3, 2), (3, 5)$. For the remaining blocks, $\kappa = 1$ instead. There is no source, and $\mathbf{f}^{\mathcal{D}} = \mathbf{0}$. A no-flow boundary condition ($\mathbf{u}^{\mathcal{D}} \cdot \mathbf{n} = 0$) is posed on the left-, right-, and bottom-sides of the domain.

The BJS coefficient $\alpha = 1$.

There is no known analytical solution for comparison, but our new finite element scheme can capture the main physics features. Shown in Fig. 3 are the velocity and pressure profiles obtained on a uniform rectangular mesh with $h = 1/20$. Here are some qualitative observations.

(i) Smooth flow exchange between the free flow (Stokes) and the porous-medium flow (Darcy) across the known interface ($y = 0$): for $x > 1$, fluid travels from the Stokes domain to the Darcy domain; for $x < 1$, fluid travels back from the Darcy domain to the Stokes domain;
(ii) Pressure singularity at the two corners $(0, 1), (2, 1)$ for Stokes flow;
(iii) Detours of flow path around the six low permeability blocks for Darcy flow.

Example 4 (*Three-Domain Coupling*)**.** This is a standard filtration example that has been tested by others in [6,13]. We test this example to show the presented methodology in this paper may be extended to more general domain couplings. We consider coupling of three domains horizontally, which may also be referred to as Stokes–Darcy–Stokes coupling. Specifically, $\Omega_1 = (-1, 0) \times (0, 1)$, $\Omega_2 = (0, 1) \times (0, 1)$, $\Omega_3 = (1, 2) \times (0, 1)$. The two interfaces are $\mathcal{I}_1 = \{x = 0\} \times (0, 1)$ and $\mathcal{I}_2 = \{x = 1\} \times (0, 1)$. Stokes flow is considered in Ω_1 and Ω_3 with $\mu = 1$. whereas Darcy flow is considered in Ω_2 with permeability $\kappa = 1$. The BJS coefficient $\alpha = 1$.

A Dirichlet boundary condition with a parabolic profile $\mathbf{u}_D = [4y(1 - y), 0]^T$ is specified on the entry ($x = -1$) and a natural boundary condition is applied downstream at $x = 2$. No-slip boundary conditions are imposed along

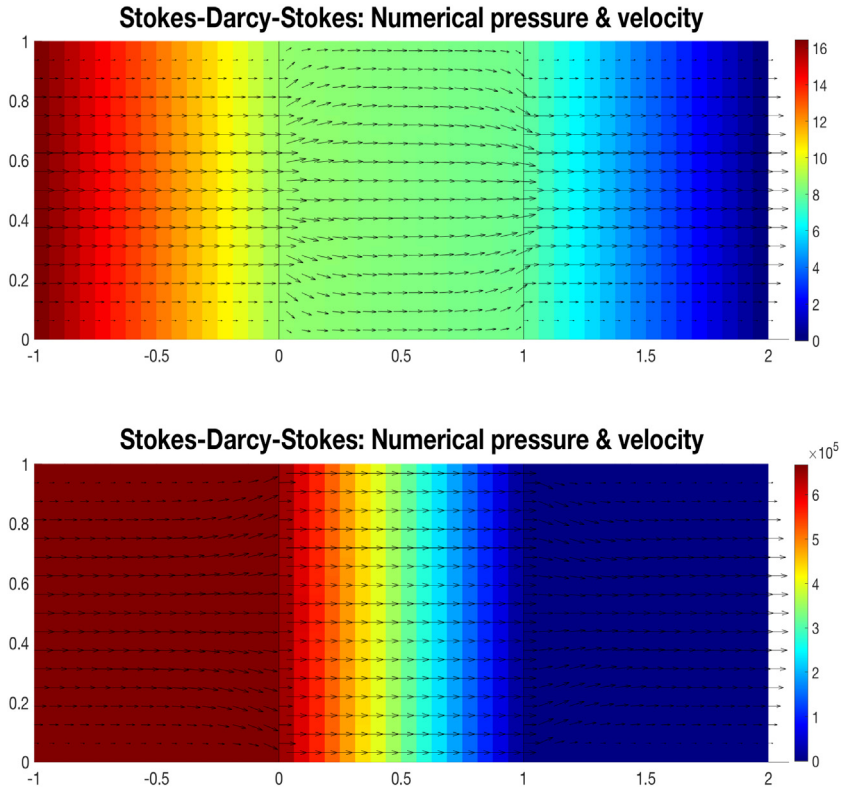

Fig. 4. Example 4 (Stokes–Darcy–Stokes coupling in three domains): Profiles of numerical velocity and pressure obtained with $h = 1/16$: (top) $\kappa = 1.0$; (bottom) $\kappa =$ 1E-6. Note Stokes velocity is plotted at nodes but Darcy velocity is plotted at element centers.

the lateral boundaries of the Stokes domains, and normal flux conditions $\mathbf{u}^{\mathcal{D}} \cdot \mathbf{n} = 0$ are applied along the lateral boundaries of the Darcy domain. All body forces and source term are set to zero.

In Fig. 4, we show the numerical results with $h = 1/16$ for the cases of $\kappa = 1.0$ (top) and $\kappa =$ 1E-6 (bottom). Comparing the two cases, we see that the magnitude of the drop in the pressure across each Stokes domain is approximately the same, but the magnitude of the pressure drop across the Darcy domain is inversely proportional to the magnitude of the permeability. In addition, we observe some slight differences in the velocity fields in the Stokes domains near the Stokes–Darcy interfaces. This is due to the fact that the tangential component of the Stokes velocity is inversely proportional to the square root of the permeability through the BJS condition.

8. Concluding remarks

In this paper, we have developed a new finite element method for coupled Stokes–Darcy problems on quadrilateral meshes that combines the classical Bernardi–Raugel element pair (BR_1, Q_0) for Stokes flow with the new weak Galerkin element $(P_0, P_0; AC_0)$ for Darcy flow. The new method has some noticeable features.

(i) As proved theoretically and demonstrated numerically, this new method has first order accuracy in the energy norm and first order accuracy for Stokes pressure in the L^2-norm.

(ii) This new finite element scheme does not use Lagrange multipliers explicitly, but the weak Galerkin edge-based pressure unknowns on the interface behave similarly to Lagrange multipliers to impose continuity of flux, as shown in Eq. (36).

(iii) This new finite element method offers local mass conservation and normal flux continuity for the Darcy flow.

(iv) This new method has fewer unknowns, compared to many other existing methods (for 2-dim problems), but is flexible in accommodation of complicated domain geometry. The total number of unknowns is

$$2\#\text{StokesNodes} + \#\text{StokesEdges} + \#\text{StokesElements} + \#\text{DarcyElements} + \#\text{DarcyEdges}.$$

The new method can be extended to 3-dim coupled Stokes–Darcy flow problems on cuboidal hexahedral meshes based on combination of the Bernardi–Raugel element pair (BR_1, Q_0) for hexahedra and the weak Galerkin element $(P_0, P_0; AT_0)$, where AT_0 is the lowest-order Arbogast–Tao space [37]. This also means that a dimension-independent implementation may be realized in a finite element library such as `deal.II`, which now contains the Bernardi–Raugel element in version 9.1 [38]. Further extension of this approach to higher order solvers is possible by using the Taylor–Hood elements or the WG$(P_k, P_k; AC_k)$ finite elements. All these are currently under our investigation and will be reported in our future work.

Declaration of competing interest

The authors declare that they have no known competing financial interests or personal relationships that could have appeared to influence the work reported in this paper.

Acknowledgments

G. Harper and J. Liu were partially supported by US National Science Foundation under grant DMS-1819252. G. Harper was also partially supported by the U.S. Department of Energy Office of Science Graduate Student Research (SCGSR) program. The SCGSR program is administered by the Oak Ridge Institute for Science and Education (ORISE) for the DOE. ORISE is managed by ORAU under contract number DE-SC0014664. All opinions expressed in this paper are the authors and do not necessarily reflect the policies and views of DOE, ORAU, or ORISE. S. Tavener was partially supported by US National Science Foundation under grant DMS-1720473. T. Wildey's work was supported by the U.S. Department of Energy, Office of Science, Early Career Research Program. This paper describes objective technical results and analysis. Any subjective views or opinions that might be expressed in the paper do not necessarily represent the views of the U.S. Department of Energy or the United States Government. Sandia National Laboratories is a multimission laboratory managed and operated by National Technology and Engineering Solutions of Sandia, LLC., a wholly owned subsidiary of Honeywell International, Inc., for the U.S. Department of Energy's National Nuclear Security Administration under contract DE-NA-0003525.

References

[1] C. Bernardi, A.Y. Orfi, A posteriori error analysis of the fully discretized time-dependent coupled Darcy and Stokes equations, Comput. Math. Appl. 76 (2018) 340–360.
[2] W. Chen, M. Gunzburger, D. Sun, X. Wang, An efficient and long-time accurate third-order algorithm for the Stokes–Darcy system, Numer. Math. 134 (2016) 857–879.
[3] M. Discacciati, E. Miglio, A. Quarteroni, Mathematical and numerical models for coupling surface and groundwater flows, Appl. Numer. Math. 43 (2002) 57–74.
[4] M. Discacciati, A. Quarteroni, Navier–Stokes/Darcy coupling: modeling, analysis, and numerical approximation, Rev. Mat. Complut. 22 (2009) 315–426.
[5] M. Gunzburger, X. He, B. Li, On Stokes–Ritz projection and multistep backward differentiation schemes in decoupling the Stokes–Darcy model, SIAM J. Numer. Anal. 56 (2018) 397–427.
[6] O. Iliev, V. Laptev, On numerical simulation of flow through oil filters, Comput. Vis. Sci. 6 (2004) 139–146.
[7] G.S. Beavers, D.D. Joseph, Boundary conditions at a naturally permeable wall, J. Fluid Mech. 30 (1967) 197–207.
[8] P.G. Saffman, On the boundary condition at the surface of a porous medium, Stud. Appl. Math. 50 (1971) 93–101.
[9] M. Discacciati, P. Gervasio, A. Giacomini, A. Quarteroni, The interface control domain decomposition method for Stokes–Darcy coupling, SIAM J. Numer. Anal. 54 (2016) 1039–1068.
[10] B. Ganis, D. Vassilev, C. Wang, I. Yotov, A multiscale flux basis for mortar mixed discretizations of Stokes–Darcy flows, Comput. Methods Appl. Mech. Engrg. 313 (2017) 259–278.
[11] E. Burman, P. Hansbo, A unified stabilized method for Stokes and Darcy's equations, J. Comput. Appl. Math. 198 (2007) 35–51.
[12] G.N. Gatica, F.A. Sequeira, Analysis of the HDG method for the Stokes–Darcy coupling, Numer. Methods Partial Differential Equations 33 (2017) 885–917.
[13] G. Kanschat, B. Riviére, A strongly conservative finite element method for the coupling of Stokes and Darcy flow, J. Comput. Phys. 229 (2010) 5933–5943.

[14] R. Li, J. Li, X. He, Z. Chen, A stabilized finite volume element method for a coupled Stokes–Darcy problem, Appl. Numer. Math. 133 (2018) 2–24.
[15] B. Riviére, I. Yotov, Locally conservative coupling of Stokes and Darcy flows, SIAM J. Numer. Anal. 42 (2005) 1959–1977.
[16] H. Rui, R. Zhang, A unified stabilized mixed finite element method for coupling Stokes and Darcy flows, Comput. Methods Appl. Mech. Engrg. 198 (2009) 2692–2699.
[17] Y. Chen, X. Zhao, Y. Huang, Mortar element method for the time dependent coupling of Stokes and Darcy flows, J. Sci. Comput. 80 (2019) 1310–1329.
[18] M. Discacciati, R. Oyarzúa, A conforming mixed finite element method for the Navier–Stokes/Darcy coupled problem, Numer. Math. 135 (2017) 571–606.
[19] G.N. Gatica, S. Meddahi, R. Oyarzua, A conforming mixed finite element method for the coupling of fluid flow with porous media flow, IMA J. Numer. Anal. 29 (2009) 86–108.
[20] G. Fu, C. Lehrenfeld, A strongly conservative hybrid DG/mixed FEM for the coupling of Stokes and Darcy flow, J. Sci. Comput. 77 (2018) 1605–1620.
[21] G. Wang, F. Wang, L. Chen, Y. He, A divergence free weak virtual element method for the Stokes–Darcy problem on general meshes, Comput. Methods Appl. Mech. Engrg. 344 (2019) 998–1020.
[22] W. Chen, F. Wang, Y. Wang, Weak Galerkin method for the coupled Darcy–Stokes flow, IMA J. Numer. Anal. 36 (2016) 897–921.
[23] R. Li, Y. Gao, J. Li, Z. Chen, A weak Galerkin finite element method for a coupled Stokes–Darcy problem on general meshes, J. Comput. Appl. Math. 334 (2018) 111–127.
[24] V. Girault, D. Vassilev, I. Yotov, Mortar multiscale finite element methods for Stokes–Darcy flows, Numer. Math. 127 (2014) 93–165.
[25] A. Caiazzo, V. John, U. Wilbrandt, On classical iterative subdomain methods for the Stokes–Darcy problem, Comput. Geosci. 18 (2014) 711–728.
[26] J. Camano, G. Gatica, R. Oyarzua, R. Ruiz-Baiere, P. Venegas, New fully-mixed finite element methods for the Stokes–Darcy coupling, Comput. Methods Appl. Mech. Engrg. 295 (2015) 362–395.
[27] C. Bernardi, G. Raugel, Analysis of some finite elements for the Stokes problem, Math. Comp. 44 (1985) 71–79.
[28] J. Liu, S. Tavener, Z. Wang, Penalty-free any-order weak Galerkin FEMs for elliptic problems on quadrilateral meshes, J. Sci. Comput. 83 (2020) 47.
[29] G. Lin, J. Liu, L. Mu, X. Ye, Weak Galerkin finite element methods for Darcy flow: Anisotropy and heterogeneity, J. Comput. Phys. 276 (2014) 422–437.
[30] J. Liu, S. Tavener, Z. Wang, Lowest-order weak Galerkin finite element method for Darcy flow on convex polygonal meshes, SIAM J. Sci. Comput. 40 (2018) B1229–B1252.
[31] F. Brezzi, M. Fortin, Mixed and Hybrid Finite Element Methods, Springer-Verlag, 1991.
[32] D.N. Arnold, D. Boffi, R.S. Falk, Quadratic $H(div)$ finite elements, SIAM J. Numer. Anal. 42 (2005) 2429–2451.
[33] T. Arbogast, M. Correa, Two families of mixed finite elements on quadrilaterals of minimal dimension, SIAM J. Numer. Anal. 54 (2016) 3332–3356.
[34] J. Liu, S. Tavener, Z. Wang, The lowest order weak Galerkin finite element methods for the Darcy equation on quadrilateral and hybrid meshes, J. Comput. Phys. 359 (2018) 312–330.
[35] T. Arbogast, G. Pencheva, M.F. Wheeler, I. Yotov, A multiscale mortar mixed finite element method, Multiscale Model. Simul. 6 (1) (2007) 319–346.
[36] D. Arnold, D. Boffi, R. Falk, Approximation by quadrilateral finite elements, Math. Comp. 71 (2002) 909–922.
[37] T. Arbogast, Z. Tao, Construction of H(div)-conforming mixed finite elements on cuboidal hexahedra, Numer. Math. 142 (2019) 1–32.
[38] D. Arndt, W. Bangerth, T.C. Clevenger, D. Davydov, M. Fehling, D. Garcia-Sanchez, G. Harper, T. Heister, L. Heltai, M. Kronbichler, R.M. Kynch, M. Maier, J.-P. Pelteret, B. Turcksin, D. Wells, The `deal.II` library, version 9.1, J. Numer. Math. (2019) Available online.